Distinct evolution of SARS-CoV-2 Omicron XBB and BA.2.86 lineages combining increased fitness and antibody evasion

Delphine Planas[1,2*], Isabelle Staropoli[1], Vincent Michel[3], Frederic Lemoine[4,5], Flora Donati[4,6], Matthieu Prot[4], Francoise Porrot[1], Florence Guivel-Benhassine[1], Banujaa Jeyarajah[6], Angela Brisebarre[6], Océane Dehan[6], William Henry Boland[1], Mathieu Hubert[1], Julian Buchrieser[1], Thibault Vanhoucke[1], Pierre Rosenbaum[7], David Veyer[8,9], Hélène Péré[8,9], Bruno Lina[10,11], Sophie Trouillet-Assant[10,11] on behalf of COVID-SER study group, Laurent Hocqueloux[12], Thierry Prazuck[12], Etienne Simon-Loriere[4,6*, $], Olivier Schwartz[1,2*, $].

[1] Virus and Immunity Unit, Institut Pasteur, Université Paris Cité, CNRS UMR3569, Paris, France.
[2] Vaccine Research Institute, Créteil, France.
[3] Pathogenesis of Vascular Infections Unit, Institut Pasteur, INSERM, Paris, France.
[4] G5 Evolutionary Genomics of RNA Viruses, Institut Pasteur, Université Paris Cité, Paris, France.
[5] Bioinformatics and Biostatistics Hub, Paris, France.
[6] National Reference Center for Respiratory Viruses, Institut Pasteur, Paris, France.
[7] Humoral Immunology Laboratory, Institut Pasteur, Université Paris Cité, INSERM U1222, Paris, France.
[8] Laboratoire de Virologie, Service de Microbiologie, Hôpital Européen Georges Pompidou, Paris, France.
[9] Functional Genomics of Solid Tumors (FunGeST), Centre de Recherche des Cordeliers, INSERM, Université de Paris, Sorbonne Université, Paris, France.
[10] Laboratoire de Virologie, Institut des Agents Infectieux, Centre National de Référence des virus des infections respiratoires, Hospices Civils de Lyon, Lyon, France.
[11] CIRI, Centre International de Recherche en Infectiologie, Team VirPath, Univ Lyon, Inserm, U1111, Université Claude Bernard Lyon 1, CNRS, Lyon, France.
[12] CHU d'Orléans, Service de Maladies Infectieuses, Orléans, France.

[*]Co-corresponding authors
delphine.planas@pasteur.fr; etienne.simon-loriere@pasteur.fr and olivier.schwartz@pasteur.fr (lead contact)
[$] co-last authors

Abstract

The unceasing SARS-CoV-2 circulation in an immune population led to the continuous emergence of new viral sublineages. Here, we isolated and characterized XBF, XBB.1, XBB.1.5, XBB.1.9.1, XBB.1.16.1, EG.5.1.1, EG.5.1.3 and BA.2.86.1 variants, that represented >80% of circulating strains as of November 2023. These XBB subvariants carry few recurrent mutations in the spike, whereas BA.2.86.1 harbors >30 additional mutations. We compared their fitness in culture, sensitivity to antivirals and sera from vaccinees. These variants replicated in IGROV-1 and no longer in VeroE6 cells. They were not markedly fusogenic. BA.2.86.1 displayed the strongest binding to ACE2. They potently infected nasal epithelial cells, with EG.5.1.3 exhibiting the highest fitness. Nirmatrelvir, Remdesivir and Molnupiravir remained active, whereas Sotrovimab lost efficacy against BA.2.86.1. Neutralizing antibody (NAb) responses from vaccinees and BA.1/BA.2-infected individuals were 7 to 21-fold lower compared to BA.1, without major differences between variants. A breakthrough XBB infection enhanced NAb responses, particularly against XBB variants. Thus, while distinct, the evolution trajectory of these variants combines increased fitness and antibody evasion.

Introduction

Succeeding sub-lineages of Omicron have spread since the appearance of BA.1 in November 2021 (Tegally et al., 2022; Viana et al., 2022). More than 90% of the human population has been probably infected by one Omicron subvariant, in the absence of an efficient and long-lasting protection against novel viral acquisitions conferred by previous infections or vaccinations (Abu-Raddad et al., 2022; Andrews et al., 2022; Kuhlmann et al., 2022; Lin et al., 2023), allowing the virus to further evolve and diversify. Identified in September 2022, the XBB lineage originated from a recombination of two BA.2-derived variants (BJ.1 and BM.1.1.1) and progressively replaced most of previous Omicron strains. Members of this lineage are characterized by enhanced transmissibility rates and extensive immune evasion properties (Miller et al., 2023; Wang et al., 2022). Collectively, these variants are responsible for small waves of contaminations in many countries. Their geographical distribution is somewhat heterogeneous. The variants are closely related and carry an additional and limited set of mutations in the spike corresponding to a stepwise accumulation of changes. Convergent evolution may have been associated with this process. For instance, many lineages independently acquired mutations in the Receptor Binding Domain (RBD) of the spike, including F486P or F456L, that are known escape mutations for neutralizing antibodies. (Barnes et al., 2020) (Gruell et al., 2022). Other recombinants increased in frequency in specific regions of the world but did not spread extensively, for example XBF (a recombinant of BA.5.2.3 and BA.2.75.3 lineages) or XBC (a recombinant of BA.2 and

Delta lineages), both noted in Australia or New Zealand and carrying the F486P substitution. This convergent evolution is likely due to a similar selective pressure exerted by imprinted or hybrid immunity triggered by SARS-CoV-2 Omicron infection and/or vaccination (Cao et al., 2022a; Crotty, 2021; Park et al., 2022b; Pulliam et al., 2022).

In August 2023, a lineage named BA.2.86 corresponding to an important evolutionary jump has been detected in multiple countries, prompting its rapid classification as a Variant under monitoring (VUM) by the World Health Organization (WHO, 2023). About 3000 cases have been reported as of November 2023. The effective reproduction number (Re) of BA.2.86 is estimated to be higher or similar than those of XBB.1.5 and EG.5.1 (Uriu et al., 2023). A high attack rate of BA.2.86 (above 85%) occurred in a large care home outbreak, confirming its high transmissibility (Reeve et al., 2023). There is so far no clinical evidence of increased pathogenicity of BA.2.86. In hamsters, BA.2.86 displays an attenuated phenotype (Herder et al., 2023) (Tamura et al., 2023). The impact of the unprecedented combination of mutations characterizing this lineage on antibody evasion has started to be deciphered. A few recent articles and preprints reported that NAb responses to BA.2.86 are lower than to BA.2, but comparable or slightly higher than to other simultaneously circulating XBB-derived variants (Faraone et al., 2023; Hu et al., 2023; Khan et al., 2023; Lasrado et al., 2023; Lassauniere et al., 2023; Qu et al., 2023; Sheward et al., 2023; Uriu *et al.*, 2023; Wang et al., 2023a; Wang et al., 2023b; Yang et al., 2023). Most of these studies were performed with lentiviral or VSV pseudotypes. Isolation of a BA.2.86 virus confirmed the antibody-escape properties of this strain (Lassauniere *et al.*, 2023). It has also been shown that the BA.2.86 spike displays stronger affinity to ACE2 than other variants (Yang *et al.*, 2023) (Wang *et al.*, 2023a), but the consequences on viral replication and tropism remain poorly understood.

Here, we isolated and characterized 8 viral strains, namely XBF, XBB.1, XBB.1.5, XBB.1.9.1, XBB.1.16.1, EG.5.1.1, EG.5.1.3 and BA.2.86.1 that were circulating in October-November 2023. We performed a side-by-side comparison of their replication in cell lines and relevant human primary nasal epithelial cells, their binding to ACE2 and fusogenicity. We also examined their sensitivity to previously approved mAbs and antiviral drugs, to sera from recipients of various vaccine regimens, and to individuals who experienced breakthrough infections during XBB circulation.

Results

Mutations in XBB-derived and BA2.86 spike sequences

XBB variants have replaced the previously circulating Omicron variants in early 2023 and have been continuously evolving. As of October 2023, the main XBB sub-variants, representing about 80% of reported viral sequences, were XBB.1.5, XBB.1.9.1, XBB.1.16, XBB.2.3 and the EG.5.1 sublineage (Fig.

1a). EG.5.1 is a descendant of XBB.1.9.2 that was designated in May 2023 and has since then been on the rise (Uraki et al., 2023). The set of the spike mutations in these variants is depicted Fig. 1b and the resulting phylogenetic tree is displayed Fig. S1a. In addition to the R346T and N460K substitutions, these most frequent XBB lineages independently acquired the S486P substitution. Other substitutions were noted at position 486 of the spike in previous variants, such as 486V in BA.5 and descendants (Fig. S1b). These variants have spread worldwide, although local variations in frequency have been noted. The subsequent sequential acquisition of the F456L substitution has been repeatedly noted in 486P carrying XBB lineages, suggesting an epidemiological advantage for these mutations and their combination in this genomic background. More than 65% of genomes shared on GISAID in October 2023 carry both F486L and F456L substitutions.

In contrast to the steady accumulation of substitutions observed in XBB sublineages, similar to the evolution observed in BA.2- and BA.5-derived lineages in 2022, the evolutionary processes that led to the emergence of BA.2.86 have not been captured. BA.2.86 and notably its spike carries a novel and distinct constellation of changes. This leads to a novel branch in the SARS-CoV-2 spike phylogenetic tree (Fig. S1a). Compared with its BA.2 ancestor, the spike contains 34 supplementary changes, a number comparable to the difference between the initial Wuhan virus and the first Omicron BA.1, including novel changes (insertion, deletions), as well as substitutions spanning the N-terminal Domain (NTD), the RBD and the S2 region (Fig. 1b). Some mutations, such as G446S, N460K, F486P, and R493Q have been previously reported in other variants (Miller *et al.*, 2023) (Yue et al., 2023) (Wang *et al.*, 2022) (Fig. S1b), but others are less frequent and poorly characterized. Furthermore, BA.2.86 has been quickly diversifying as it spreads. BA2.86.1 is for instance characterized by the acquisition of two novel mutations in ORF1.

Isolation of XBB.1.5, XBB.1.9.1, XBB.1.16.1, XBF, EG.5.1.1, EG.5.1.3 and BA.2.86.1 variants.

We isolated XBB.1, XBB.1.5, XBB.1.9.1, XBB.1.16.1, XBF, EG.5.1.1, EG.5.1.3 and BA.2.86.1 variants from nasopharyngeal swabs received at the French National Reference Center of Respiratory viruses (Paris, Lyon) and Hôpital Européen Georges Pompidou (Paris, France), using either a Vero E6 TMPRSS2+ clone (thereafter termed Vero E6 TMP-2 cells) or IGROV-1 cells as targets. We recently reported that the IGROV-1 human ovarian cell line is highly sensitive to SARS-CoV-2 and rapidly produces high levels of infectious virus (Planas et al., 2023). After isolation, the 8 viruses were thus amplified by one passage on IGROV-1 cells. The sequences of the variants after amplification were identical to those obtained from the primary samples (GISAID accession numbers are indicated in Table S3), indicating that no mutations occurred during this short culture period. The spike mutations in these 8 variants, compared to BA.2, are depicted in Fig. 1b. We also compared the spike mutations of a larger panel of variants to the Wuhan ancestral strain in Fig. S1b.

Replication of XBB-derived and BA2.86 variants in Vero E6 derivatives and IGROV-1 cells.

We characterized the fitness of the 8 variants by assessing their replication in different cell types and compared them to either D614G, BA.1, BA.5 or BQ.1.1. We first chose Vero E6 and IGROV-1 cells, that both naturally express ACE2, but not TMPRSS2, the serine protease that primes the SARS-CoV-2 for fusion, as verified by flow cytometry (Fig. S2). Vero E6 cells are known to efficiently replicate pre-Omicron strains but are less sensitive to previous Omicron variants (Planas *et al.*, 2023). We thus compared the permissibility of Vero E6 and IGROV-1 cells to this set of variants (Fig. S3a). Viral stocks were serially diluted and incubated with the two target cells. After 48h, cells were stained with an anti-SARS-CoV-2 N monoclonal antibody. Foci of infected cells were scored with an automated confocal microscope (Fig. S3b). The ancestral D614G strain was similarly infectious in the two cell lines (Fig. S3). In contrast, none of the 11 Omicron variants efficiently infected Vero E6 cells whereas they were highly infectious for IGROV-1 cells. We then asked whether the poor infectivity of the variants in Vero E6 was due to the lack of TMPRSS2. We thus selected two Vero E6 subclones engineered to express TMPRSS2. The first clone (termed Vero E6 TMP-1) was generated in our laboratory (Planas *et al.*, 2023) and expresses high levels of TMPRSS2 and rather low levels of ACE2, probably because this receptor can be cleaved by the protease (Heurich et al., 2014) (Fig. S2). The Vero E6 TMP-2 was previously described (Matsuyama et al., 2020). It expresses low surface levels of TMPRSS2 and ACE2 levels comparable to those in parental Vero E6 cells (Fig. S2). We thus compared the kinetics of viral replication in IGROV-1, Vero E6, Vero E6-TMPRSS2 clones 1 and 2. We used as controls Delta and BQ.1.1 (a BA5-derived Omicron variant), and compared them to XBB.1, XBB.1.5, EG.5.1.3 and BA.2.86.1 (Fig. 2a). All viruses efficiently replicated in IGROV-1 cells, with a peak of infected cells being detected at day 2 post infection (p.i.). The Omicron variants did not potently infect Vero E6 during the 4-day survey period. The two Vero E6-TMPRSS2 clones behave differently regarding their sensitivity to these variants. Vero E6 TMP-1 did not support strong replication of Omicron variants, despite allowing growth of Delta. In contrast, Vero E6 TMP-2 efficiently replicated the novel variants (Fig. 2a). The differences between Vero E6 TMP-1 and Vero E6 TMP-2 might be due to clonal effects. Alternatively, the high levels of TMPRSS2, associated with reduced surface expression of ACE2 in Vero E6 TMP-1 might be detrimental for the replication of XBB-derived and BA.2.86.1 variants. Regardless of the underlying mechanisms, our results indicate that the recent XBB-derived and BA.2.86 variants display a different tropism than pre-Omicron viruses for some cell lines. Low expression of TMPRSS2 in Vero E6 cells is associated with permissibility of the cells to XBB-derived and BA.2.86.1 infection.

We further explored the mechanisms underlying the high sensitivity of IGROV-1 to SARS-CoV-2 replication. To this aim, we examined viral entry pathways in these cells and performed infections in presence of either Camostat, a TMPRSS2 inhibitor, SB412515, a cathepsin L inhibitor, or E-64d, a pan-

cysteine protease inhibitor acting mainly on endocytic proteases (Koch et al., 2021) (Meng et al., 2022). The drugs were added 2 h before infection and maintained for 24 h. Infections were revealed by scoring the area of N+ infected cells (Fig. S4). We selected a few pre-Omicron and recent Omicron variants, (D614G, Delta, BA.1, XBB.1 and XBB.1.16.1) and tested the effect of the drugs in IGROV-1, Vero E6 and Vero TMP-1 cells. Camostat (at 100 µM) did not inhibit viral replication in IGROV-1 and Vero E6 cells, in line with the absence of detection of TMPRSS2 in these cells by flow cytometry. Camostat inhibited viral replication by 50-80% in Vero E6 TMP-1 cells, confirming that TMPRSS2 facilitates viral entry when present in target cells. There was no significant difference between the variants in their sensitivity to Camostat in Vero E6 TMP-1 cells. SB412515 and E-64d (both at 10 µM) strongly inhibited viral infections in IGROV-1 cells (>90% inhibition for all variants) but were globally less efficient in Vero E6 cells (Fig. S4). This strongly suggests that endocytic viral entry is particularly active in IGROV-1. With both SB412515 and E-64d, similar ED50 were obtained for D614G, XBB.1.5, EG.5.1.3 and BA.2.86.1 variants, which may indicate that all variants use similar entry pathways in IGROV-1 cells (Fig. 2b). In contrast to their strong antiviral effect in IGROV-1 and to a lower activity in Vero E6 cells, SB412515 and E-64d were almost inactive in Vero E6 TMP-1 cells, confirming that when TMPRSS2 is present, viral entry and fusion preferentially occurs at the cell surface (Koch *et al.*, 2021) (Mykytyn et al., 2023).

Therefore, IGROV-1 are highly sensitive to all SARS-CoV-2 strains, most likely because of a strong endocytic pathway facilitating viral entry after internalization.

Fusogenicity and ACE2 binding of XBB-derived and BA2.86 variants.

We next investigated the fusogenicity of the variant spike proteins and their ability to form syncytia independently of viral replication. We used a GFP-Split based model in which fused cells become GFP+ (Fig. 3a) (Buchrieser et al., 2020) (Rajah et al., 2021). We transfected the corresponding spikes into 293T cells expressing the GFP-11 subunit and co-cultivated them with IGROV-1 cells expressing the GFP1-10 subunit for 18 h (Fig. 3a). Spike expression on transfected HEK293T cells was similar across variants, as measured by staining with a pan-coronavirus anti-S2 mAb (Fig. S5). As previously reported by us and others, the ancestral D614G and Delta strains were more fusogenic than the early Omicron BA.1 and BA.4/5 variants (Bolland et al., 2023) (Planas *et al.*, 2023) (Meng *et al.*, 2022) (Suzuki et al., 2022). BQ.1.1 and XBB.1.5/XBB.1.9 spikes partially regained fusogenicity, whereas XBB.1.16 and the more recent EG.5.1 and BA.2.86 spikes displayed a lower fusogenic potential than BA.4/5 spike (Figure 3b,c). This profile of fusogenicity was similarly observed when Vero E6 cells were used as targets (Fig. 3d). With Vero E6 TMP-1 as target cells, the number of syncytia was increased by about 2-fold for all variants, when compared to parental Vero E6 cells (Fig. 3d), indicating that TMPRSS2 enhances their fusogenic activity. Altogether, these results indicate that the recent XBB-

derived and BA.2.86 variant spikes do not display high fusion properties, when compared to Delta or to their Omicron predecessors, at least in the cell lines tested.

We next examined the affinity of the different variant spikes to ACE2. To this aim, we infected IGROV-1 cells with the panel of variants for 24h. Cells were then stained with an anti- SARS-CoV-2 N antibody to visualize productively infected cells, and to serial dilutions of soluble biotinylated ACE2 that was revealed with fluorescent streptavidin and analyzed by flow cytometry (Fig. S6a). ACE2 titration binding curves were generated, and EC50 (the amount of ACE2 needed for 50% binding) was calculated (Fig. S6b). The spikes of XBB.1, XBB.1.16.1 and EG.5.1.3 had lower affinities to ACE2 than BA.1, whereas BA.2.86 had the highest affinity to ACE2 (Fig. 3e). We obtained similar results when we examined the binding of soluble ACE2 to 293T cells transiently expressing the different spikes (Fig. 3f, confirming recent reports obtained in spike-transfected cells or with recombinant proteins (Yang *et al.*, 2023) (Wang *et al.*, 2023a).

Replication of XBB-derived and BA2.86 variants in primary nasal epithelial cells.

We then used primary nasal epithelial cells (hNEC) grown over a porous membrane and differentiated at the air–liquid interface for 4 weeks (from MucilAirB^{TM}), to compare the different variants in a relevant model of SARS-CoV-2 infection (Mlcochova et al., 2021) (Robinot et al., 2021) (Suzuki *et al.*, 2022). The cells were infected with each variant at a similar low viral inoculum (100 µl of viral stocks containing 2x10^{3} infectious units/ml). As previously reported (Mlcochova *et al.*, 2021; Willett et al., 2022) (Suzuki *et al.*, 2022) (Bolland *et al.*, 2023), BA.1 replicated faster than Delta and D614G, as quantified by viral RNA release monitored every day up to 4 days pi (Fig. 4a, b). Compared to Delta, there was up to 60-fold increase in viral RNA levels measured at 24 h pi for BA.1. The recent XBB-derived variants also exhibited a replication advantage compared to BA.1, with EG.5.1.3 displaying a 16-fold increase in average RNA release after 24 h of infection. BA.2.86.1 replication kinetics resembled those of BA.1 and were not higher than other XBB-derived variants (Fig. 4a, b). Infectious virus release was monitored at 48 h p.i. (Fig. 4c) and correlated with the viral RNA levels. We assessed by immunofluorescence the cytopathic effect induced by the different variants. Infected hNEC were stained at day 4 p.i. with anti-SARS-CoV-2 N antibodies, phalloidin (to visualize F-actin), anti-alpha tubulin antibodies (to visualize cilia) and anti-cleaved caspase 3 antibodies (to visualize apoptotic dying cells). When compared to Delta or BA.1, EG.5.1.3 and BA.2.86.1 displayed elevated markers of cytopathy, including disappearance of the ciliated structure and activation of caspase 3 (Fig. 4d).

Therefore, the XBB-derived variants are globally more infectious in hNECs compared to their predecessors, with EG.5.1.3 being the fittest. EG.5.1.3 and BA.2.86.1 variants displayed marked cytopathy in these cells.

Sensitivity of XBB-derived and BA2.86 variants to antiviral antibodies and small molecules.

Several anti-spike monoclonal antibodies (mAbs) have been used as pre- or post-exposure therapy in individuals at risk for severe disease (Gruell *et al.*, 2022). However, the first Omicron variants BA.1, BA.2 and BA.5 escaped neutralization from most of the mAbs, leading to changes in treatment guidelines (WHO, 2022). For instance, as of mid-2022 and later, Ronapreve (Imdevimab + Casirivimab) or Evusheld (Cilgavimab + Tixagevimab) cocktails and Sotrovimab were no longer approved (WHO, 2022). However, Sotrovimab retains some neutralizing and non-neutralizing Fc-mediated functions against BQ.1.1 and XBB.1.5 (Bruel et al., 2023). We thus assessed with the S-Fuse assay the sensitivity of D614G, XBB.1.16.1, EG.5.1.3 and BA.2.86.1 to Ronapreve, Evusheld or Sotrovimab. We included the ancestral D614G strain as a control, which was efficiently neutralized by the mAbs (Fig. 5a). Evusheld and Ronapreve combinations were inactive against XBB.1.16.1, EG.5.1.3 and BA2.86.1 variants. Sotrovimab remained weakly functional against XBB.1.16.1 and EG.5.1.3 but lost antiviral activity against BA.2.86.1. We then examined whether the neutralization profile of Sotrovimab correlated with the ability of the mAb to bind the different spikes. To this aim, we measured by flow cytometry the binding of Sotrovimab to IGROV-1 cells infected with the corresponding variants (Fig. S7a,b). Cells were stained with the pan coronavirus S2 antibody mAb10 as a control (Fig. S7c). Sotrovimab bound to all XBB-derived variants but not to BA.2.86.1. This is likely due at least to the presence of the K356T mutation in BA.2.86.1 RBD, that has been previously identified as conferring resistance to Sotrovimab (Addetia et al., 2023) (Ragonnet-Cronin et al., 2023).

We then assessed the efficacy of the currently approved anti-SARS-CoV-2 drugs Nirmatrelvir (present in Paxlovid), Remdesivir and Molnupiravir against D614G, XBB.1.5.1, EG.5.1.3 and BA.2.86.1. IGROV-1 cells were exposed to serial dilutions of the compounds, exposed to the variants, and infection was revealed after 24 h (Fig. 5b. The antiviral molecules remained active against the tested variants, with no significant differences in their EC50.(10 nM, 3.4 µM and 0.04 nM for Nirmatrelvir, Molnupiravir and Remdesivir, respectively).

Cohort design

We collected 75 sera from two different cohorts representing a total of 41 vaccinated and/or infected individuals. The characteristics of the participants (dates of vaccination, breakthrough infection and sampling) are indicated in Table S1.

The first cohort includes two groups of individuals. The first group is composed of 21 health-care workers, in Orleans, France (Table S1a). The participants received two doses of Pfizer BNT162b2 vaccine and one or two booster doses with the same monovalent vaccine. 15 out of 21 individuals experienced a pauci-symptomatic breakthrough infection after the third injection. We did not generally identify the Omicron subvariant responsible for the breakthrough infections. 14 individuals

were infected between December 2021 and mid-June 2022, a period when BA.1 and BA.2 were successively dominant in France (France, 2022). One individual was infected in August 2022 and was likely positive for BA.5. All individuals received a Bivalent Wuhan/BA.5 Pfizer boost between December 2022 and February 2023. The second group includes 12 vaccinated health-care workers, in Orleans, France, that experienced a breakthrough Omicron infection in August/September 2023, when XBB-derived variants were predominant (Table S1c).

The second cohort includes 8 health-care workers, in Lyon, France, that were longitudinally sampled at day 0, one month and 6 months after their Bivalent Wuhan/BA.5 Pfizer boost (Table S1b).

Sensitivity of XBB-derived and BA2.86.1 variants to sera from vaccinees.

We assessed the sensitivity of the panel of XBB-derived and BA2.86.1 variants to serum samples from the three cohorts described above. We first asked whether antibodies elicited by three doses of the original Pfizer vaccine neutralized the novel Omicron subvariants. Twenty-one individuals were analyzed 12 months post third dose (from cohorts 1 and 2, Table S2a). Among them, 12 individuals experienced a BA.1/BA.2 breakthrough infection. We measured the potency of their sera against BQ.1.1, XBB.1, XBB.1.5; XBB.1.9.1, XBB.1.16.1, XBF, EG.5.1.3 and BA.2.86.1. We used as reference the D614G ancestral strain, as well as BA.1 and BA.5 (Fig. 6a). We calculated the ED50 (Effective Dose 50%) for each combination of serum and virus. The ED50 were high for D614G (ED50 of $6.7x10^3$) and were decreased by 5-fold for BA.1 and BA.5, confirming the escape properties of these previous sublineages (Planas *et al.*, 2023). With the XBB-derived strains, the ED50 were low, ranging from $2x10^2$ to $8x10^1$. XBB.1.16.1 and EG.5.1.3 neutralization titers were the lowest (22 and 30-fold lower than BA.1, respectively). BA.2.86.1 neutralization was about 2-fold more sensitive to neutralization than EG.5.1.3, confirming recent results (Faraone *et al.*, 2023; Hu *et al.*, 2023; Khan *et al.*, 2023; Lasrado *et al.*, 2023; Lassauniere *et al.*, 2023; Qu *et al.*, 2023; Sheward *et al.*, 2023; Uriu *et al.*, 2023; Wang *et al.*, 2023a; Wang *et al.*, 2023b; Yang *et al.*, 2023).

We then asked how a boost with the bivalent original/BA.5 Pfizer mRNA vaccine modified these humoral responses. Sera from 20 and 15 individuals of the two cohorts were tested one month (Table S2b) and six months (Table S2c) after the bivalent boost, respectively (Fig. 6b). After one month, titers were increased against all the variants tested, when compared to individuals that did not receive the bivalent boost (Fig. 6a,b). The highest responses were detected against D614G, and to a lower extent to BA.1 and BA.5, reflecting a probable imprinting of the immune response. The responses against the recent XBB-derived and BA.2.86 variants remained about 10-25 fold lower than against BA.5. A similar trend was observed six months after the bivalent boost. Neutralization was reduced against all strains, highlighting the declining humoral response (Planas et al., 2022a; Planas et al., 2022b). The neutralizing activity was barely detectable against XBB.1.16.1, EG.5.1.3 and BA.2.86.1 (Fig.

6c). We confirmed the stimulation and subsequent decline of the response elicited by the bivalent boost by longitudinally analyzing 15 individuals, tested before and one, three and six months after vaccine administration. The neutralizing titers peaked at one month and then progressively declined over time (Fig. 6d).

Altogether, these results indicate that the XBB-derived and BA.2.86.1 variants are poorly neutralized by sera from individuals having received 3 doses of the original monovalent vaccine. A bivalent boost increased neutralizing titers, which remained however low with EG.5.1.3 and BA.2.86.1.

Impact of XBB breakthrough infections on neutralization.

We then examined the impact of breakthrough infections on the cross-neutralizing activity of serum antibodies. We analyzed the sera from twelve individuals that were infected in September 2023 (Table S2d), at a time where the main variants circulating in France were XBB.1.9*, XBB.2.3* and XBB.1.16* (representing 49%, 20%, and 14% of the sequenced cases respectively) (GISAID https://www.epicov.org). Samples were analyzed about 3 weeks post-infection (median 19 days; range 10-50 days). A strong augmentation of neutralization against all viruses tested was observed, with ED50 between $1.5x10^3$ to $1.4x10^4$ (Fig. 6e). Compared to BA.1, the Nab titers were reduced by about 4-fold against EG.5.1.3 and BA.2.86.1 (ED50 of $2x10^3$, respectively). Therefore, post-vaccination breakthrough infection during circulation of XBB-related viruses led to an increase in neutralizing antibody titers, with reduced disparities between variants. This suggests that the anamnestic humoral response triggered by XBB infection includes both a recall of a B-cell memory and the induction of a cross-neutralizing immunity.

Discussion

We show here that the predominant SARS-CoV-2 Omicron variants circulating in the fall 2023 have progressed towards both increased fitness, as visible in primary human cell cultures, and enhanced immune evasion properties. Independently, a novel variant has emerged, similarly presenting high fitness and immune evasion despite a distinct constellation of changes. The tropism of the recent variants for cell lines has also changed. Vero E6 cells no longer allowed efficient replication of EG.5.1.1, EG.5.1.3 and BA.2.86.1 strains. The addition of TMPRSS2 did not necessarily increase replication of these recent strains in Vero E6 cells, as illustrated by the discrepant results obtained with Vero E6 TMP-1 and Vero E6 TMP-2 clones. Clonal specificities may explain the differences of sensitivity of the two cell clones. However, an efficient viral replication occurred in Vero E6 TMP-2 cells, that express low levels of TMPRSS2, and not in Vero E6 TMP-1, that express high levels of TMPRSS2. This protease cleaves and primes the spike for fusion, but also cleaves ACE2 (Heurich *et al.*, 2014). Initial SARS-CoV-2 variants used both cleaved and uncleaved ACE2 as a receptor, whereas a shift towards

preferential use of uncleaved ACE2 for Omicron variants has been proposed (Aggarwal et al., 2023). Our results strongly suggest that a delicate balance between ACE2 and TMPRSS2 levels is necessary for optimal replication of recent variants in Vero E6 cells.

We previously reported that IGROV-1 cells are highly permissive to previous SARS-CoV-2 strains (Planas *et al.*, 2023). We extend here this observation to the recent XBB-derived and BA.2.86.1 strains and explore the underlying mechanisms. Another study confirmed the sensitivity of IGROV-1 cells to SARS-CoV-2 and reported that the cells are not defective in their interferon response to infection (Yousefi et al., 2023). We show that IGROV-1 cells naturally express ACE2 but are negative for TMPRSS2, using a selective and sensitive anti-TMPRSS2 nanobody that we recently produced (Saunders et al., 2023). Moreover, the TMPRSS2 inhibitor Camostat did not impair SARS-CoV-2 infection in IGROV-1 but was active in Vero E6 TMP-1 cells, confirming the absence of TMPRSS2 in IGROV-1 cells. In contrast, two cathepsin inhibitors, SB412515 and E-64d strongly inhibited viral infection in IGROV-1, but acted poorly in Vero E6 cells and were inefficient in Vero E6 TMP-1 cells. Our results indicate that the high permissibility of IGROV-1 to all SARS-CoV-2 strains is likely due to a particularly efficient endocytic viral entry pathway that does not rely on TMPRSS2.

We further study the fusogenicity and receptor binding properties of the variant spikes. The EG.5.1 and BA.2.86 spikes were not more fusogenic than BA.1 and BA.4/5 spikes, and even less than BQ.1.1 and XBB.1.5. The selective advantage of the most recent variants is thus not associated to an increased ability to fuse and to form syncytia, at least in the cell lines tested. Addition of TMPRSS2 in target cells similarly increased fusion with the different variant spikes, indicating that they remain sensitive to the protease. The BA.2.86 spike expressed at the surface of infected cells bound with higher efficiency to ACE2 than EG.5.1.3 and XBB.1.16.1 (3.5-fold and 4.3-fold decrease in EC50, respectively). This confirms recent results obtained with recombinant spike proteins and might be linked to a better exposure of the BA.2.86 RBD than those of XBB-derived or EG.5.1 strains (Wang *et al.*, 2023a). This increased affinity may contribute to immune escape by itself. In addition, it has been proposed that variants with high affinity for ACE2 may have a stronger evolutionary potential as they could tolerate more immune escape mutations in the RBD despite their negative impact on ACE2 binding, and thus on the overall fitness.

Both XBB.1-derived variants and BA.2.86.1 rapidly and potently replicated in primary nasal epithelial cells, amplifying a trend already observed with previous Omicron variants (Cao et al., 2022b; Meng *et al.*, 2022). This efficient replication was previously associated with a greater dependency of Omicron on endocytic entry and a lower usage of TMPRSS2 in these cells (Cao *et al.*, 2022b; Meng *et al.*, 2022), although this last point remains debated (Mykytyn *et al.*, 2023). We show here that as soon as 24 h pi, viral RNA release of the recent variants was up to 380-fold higher than Delta, and 6-fold higher than BA.1. Among the recent variants, EG.5.1.3 was the fitter and faster in these cells. The

cytopathic effect was particularly marked with both EG.5.1.3 and BA.2.86.1. Infection with these two variants was associated with a strong disappearance of cilia, a phenomenon described with other strains (Robinot *et al.*, 2021), and with activation of the caspase pathway. This accelerated and enhanced replication in a primary human tissue likely represents an important factor explaining the selective advantage and improved transmissibility of the variants. Future work will help determining how ACE2 affinity, entry pathways, TMPRSS2 usage by the spike, likely involving distinct combinations of changes in XBB lineages and BA.2.86, as well as mutations in other viral proteins are regulating viral fitness in this relevant in vitro model.

The antiviral drugs Paxlovid, Remdesivir and Molnupiravir remain active against XBB-derived and BA.2.86 variants, indicating that this therapeutic arsenal is so far not impacted. However, there is no approved mAb remaining on the market. We further show that Sotrovimab, which retained partial antiviral activity against BQ.1.1 and XBB.1.5 (Bruel *et al.*, 2023), poorly acts on EG.5.1.3 and no longer binds or inhibits BA.2.86. This novel lineage carries numerous mutations known to allow mAb evasion (Wang *et al.*, 2023a), including the K356T substitution conferring resistance to Sotrovimab (Addetia *et al.*, 2023) (Ragonnet-Cronin *et al.*, 2023). Novel mAbs are under pre-clinical and clinical development (Cao *et al.*, 2022a; Moriyama et al., 2023; Park et al., 2022a). It will be worth carefully scrutinizing their antiviral activity against BA.2.86 and other emerging subvariants.

We report that sera from individuals who had received three doses of COVID-19 Pfizer BNT162b2 vaccine displayed almost no neutralization activity against the recent XBB-derived or BA.2.86 variants. Bivalent boosters increased neutralization titers but only for an abbreviated period of time. Six months after the boost, the efficacy of the sera against EG.5.1.3 and BA.2.86.1 was barely detectable. This confirm different reports indicating that these two variants are among the most immune evasive viruses described so far, even if some variations between studies and countries have been observed (Faraone *et al.*, 2023; Hu *et al.*, 2023; Khan *et al.*, 2023; Lasrado *et al.*, 2023; Lassauniere *et al.*, 2023; Qu *et al.*, 2023; Sheward *et al.*, 2023; Uriu *et al.*, 2023; Wang *et al.*, 2023a; Wang *et al.*, 2023b; Yang *et al.*, 2023).

We further show that breakthrough infections that occurred in September 2023, during circulation of XBB variants, triggered a broader cross-neutralizing response than bivalent boosters. The differences between variants were reduced, XBB.1, EG.5.1 and BA.2.86 neutralization was globally similar in individuals who experienced such XBB breakthrough infections. Therefore, in addition to imprinted memory, other mechanisms linked to hybrid immunity, such as the generation of responses targeting novel antigens can be efficacious. This suggests that the currently approved monovalent XBB.1.5 vaccines may similarly elicit antibody responses targeting EG.5.1 and BA.2.86 variants. A preprint reported the elicitation of a cross-reactive immune response, 15 days after administration of an XBB.1.5 containing monovalent mRNA vaccine (Chalkias et al., 2023). Neutralization titers were

however lower against all XBB-derived and BA.2.86 variants than against BA. 4/5. There is a debate about the interest of annually administrating vaccines based on the circulating variants, especially in healthy individuals (Krammer and Ellebedy, 2023). It will be important to analyze the longevity of the humoral response generated by the recent XBB.1.5-based vaccines, and its link with the duration of clinical efficacy against severe forms of the disease.

There are limitations to our study. Firstly, we analyzed a limited number of serum samples. However, the marked differences between variants and groups of individuals allowed statistical analysis. Secondly, this work did not include other emerging XBB sublineages showing further evidence of convergent evolution and increasing in frequency. Multiple lineages (e.g. GK.1.1 or JD.1.1 from XBB.1.5; HK.3 or JG.3 from XBB.1.9.2; JF.1 from XBB.1.16; or DV.7.1 from BA.2.75) have independently acquired the F455L substitution in addition to F486P and F456L. Another BA.2.86 sublineage termed JN.1 is rapidly increasing in frequency in Europe and is characterized by a different amino acid substitution at the same position, F455S. Thirdly, we did not explore the role of individual mutations within the spike or in other viral proteins known to have changed in Omicron variants (Bouhaddou et al., 2023). Further research to investigate the mechanisms associated with the modifications of viral properties described here will be relevant in understanding the processes underlying the evolution of SARS-CoV-2.

In summary, we show that SARS-CoV-2 Omicron variants continuously evolve in a context of an immune human population. The selective advantage of EG.5.1 and BA.2.86 variants combines both convergent increased fitness and replication in respiratory cells, and resistance to the most prevalent antibodies.

Materials & Methods

Our research fulfills all relevant ethical requirements. An informed consent was obtained from all participants. No statistical methods were used to predetermine sample size and the experiments were not randomized. The investigators were not blinded. Sex or gender analysis was not performed due to the limited number of participants.

Cohorts

Serum from bivalent Wuhan/BA.5 Pfizer vaccine recipients or from infected individuals (Orléans, France).

The Neutralizing Power of Anti-SARS-CoV-2 Serum Antibodies (PNAS) cohort is an ongoing prospective, monocentric, longitudinal, observational cohort clinical study aiming to describe the kinetics of neutralizing antibodies after SARS-CoV-2 infection or vaccination (ClinicalTrials.gov identifier: NCT05315583). The cohort takes place in Orléans, France and was previously described

(Bruel et al., 2022b). This study was approved by the Est II (Besancon) ethical committee. At enrollment, written informed consent was collected, and participants completed a questionnaire that covered sociodemographic characteristics, clinical information and data related to anti-SARS-CoV-2 vaccination.

Serum from bivalent Wuhan/BA.5 Pfizer vaccinated individuals from Lyon, France.

A prospective, multicentric, longitudinal, interventional cohort clinical study (COVID-SER) is conducted at Hospices Civils de Lyon with the objective to evaluate the effectiveness of commercially developed serological test kits currently in development, which will be used for the diagnosis of patients with suspected SARS-CoV-2 infection. The COVID-SER-VAC ancillary study where blood samples was collected at the time of the injection(s) as per the recommended vaccination schedule was conducted (ClinicalTrials.gov identifier: NCT04341142) (Trouillet-Assant et al., 2020). A sub-study aimed to build a collection of biological samples and transfer of residual blood products to external partners for the advancement of scientific knowledge on SARS-CoV-2. We had access to 23 serum samples from hospital staff who were vaccinated with the bivalent Pfizer vaccine. Samples were taken at the time of the injection, 1 month, and 6 months after the injection At enrollment, written informed consent was collected. Virological findings (SARS-CoV-2 RT–qPCR results, date of positive test, screening, or sequences results) and data related to SARS-CoV-2 vaccination (brand product, date of first, second, third and fourth vaccination) were also collected.

Virus strains

The D614G, Delta, BA.1, BA.5 and BQ.1.1 and XBB.1.5 strains have been previously described (Bruel et al., 2022a; Bruel *et al.*, 2023; Planas *et al.*, 2023; Planas et al., 2021b).

The XBB.1 strain (hCoV-19/France/PAC-HCL022171892001/2022) strain was supplied by the National Reference Centre for Respiratory Viruses hosted by the Hôpital de la Croix-Rousse (Lyon, France) and headed by Dr Bruno Lina.

The XBB.1.9.1 strain (hCoV-19/France/GES-IPP08594/2023) was supplied by the National Reference Centre for Respiratory Viruses hosted by Institut Pasteur (Paris, France) The human sample from which strain hCoV-19/France/GES-IPP08594/2023 was isolated, was provided by Dr Djoubi from Massif des Vosges Hospital (France).

The XBB.1.16.1 strain (hCoV-19/France/GES-IPP07712/2023) was supplied by the National Reference Centre for Respiratory Viruses hosted by Institut Pasteur. The human sample was provided by Dr Vanessa Cocquerelle from Laboratory Deux Rives (France).

The XBF strain (hCoV-19/France/IDF-APHP-HEGP-81-10-2332993394/2023) was isolated from a nasopharyngeal swab of individuals attending the emergency room of Hôpital Européen Georges Pompidou (HEGP); Assistance Publique, Hôpitaux de Paris.

The EG.5.1.1 strain (hCoV-19/France/GES-IPP15954/2023) was supplied by the National Reference Centre for Respiratory Viruses hosted by Institut Pasteur. (The human sample was provided by Dr Valérie Herzig from Laboratoire Lenys, Colmar (France).

The EG.5.1.3 strain (hCoV-19/France/BRE-IPP15906/2023) was supplied by the National Reference Centre for Respiratory Viruses hosted by Institut Pasteur (Paris, France) The human sample was provided by Dr F. Kerdavid from Laboratoire Alliance Anabio, Melesse (France).

The BA.2.86.1 strain (hCoV-19/France/IDF-IPP17625/2023) was supplied by the National Reference Centre for Respiratory Viruses hosted by Institut Pasteur. The human sample was provided by Dr Aude Lesenne from Cerballiance, Lisses (France).

All patients provided informed consent for the use of their biological materials. Viral strains were amplified through one or two passages on Vero E6, Vero E6 TMPRSS2, or IGROV-1 cells. Supernatants were harvested two or three days after viral exposure. The titration of viral stocks was performed on S-Fuse cells (Buchrieser *et al.*, 2020; Planas *et al.*, 2023). Viral supernatants were sequenced directly from nasopharyngeal swabs and after isolation and amplification on Vero E6 or IGROV-1 cells.

For sequencing, an untargeted metagenomic sequencing approach was used, including ribosomal RNA (rRNA) depletion. In brief, RNA was extracted using the QIAamp Viral RNA extraction kit (Qiagen) with the provided poly-A RNA carrier. Prior to library construction, carrier RNA and host rRNA were depleted using oligo(dT) and custom probes, respectively. The resulting RNA from selective depletion was utilized for random-primed cDNA synthesis with SuperScript IV RT (Invitrogen). Second-strand cDNA was generated using Escherichia coli DNA ligase, RNase H, and DNA polymerase (New England Biolabs), and then purified with Agencourt AMPure XP beads (Beckman Coulter). Libraries were prepared using the Nextera XT kit and sequenced on an Illumina NextSeq500 platform (2 × 75 cycles). Reads were assembled using Megahit v1.2.9. The sequences have been deposited on the GISAID EpiCoV database (Table S3).

Cell lines

IGROV-1, Vero E6 and Vero E6 TMPRSS2 clone 1 (Vero E6 TMP-1) and S-Fuse cells were described previously (Buchrieser *et al.*, 2020) (Planas *et al.*, 2023). Vero E6 TMP-2 cells were kindly provided by Dr Makoto Takeda lab (Matsuyama *et al.*, 2020). 293T (CRL-3216) and U2OS (Cat# HTB-96) cells were obtained from ATCC. Cells regularly tested negative for mycoplasma.

Infection of IGROV-1, Vero E6, Vero E6 TMP-1 and Vero E6 TMP-2 cells

Six hours before infection, 30,000 cells were seeded in a µClear black 96-well plate (Greiner Bio-One). Cells were then infected with the indicated strains of SARS-CoV-2, as described in legend of Figures 2 and S2 (specifying the variants and quantities of virus used). At 24, 48, 72 or 96 h post-

exposure, the cells were fixed using 4% PFA (Electron microscopy cat# 15714-S). The cells were then intracellularly stained with anti-SARS-CoV-2 nucleoprotein (N) antibody NCP-1 (0.1 µg/mL) as described (Planas *et al.*, 2023). This staining was carried out in PBS with 0.05% saponin 1% BSA, and 0.05% sodium azide for 1 h. the cells were washed twice with PBS and stained with anti-IgG Alexa Fluor 488 (dilution 1:500, Invitrogen; cat# A11029) for 30 minutes before being washed twice with PBS. Hoechst 33342 (Invitrogen, cat# H3570) was added during the final PBS wash. Images were captured using an Opera Phenix high-content confocal microscope (PerkinElmer). The N-positive area and the number of nuclei were quantified using Harmony Software v4.9 (PerkinElmer).

Test of Antiviral molecules.

Cells were seeded in a µClear black 96-well plate (Greiner Bio-One) and pretreated for 2 hours with Camostat (Sigma, cat# E8640), E-64d (Sigma, cat# SML0057), SB412515 (Cayman Chemical, cat# 23249), Nirmatrelvir (MedChemExpress; cat# HY-138687), Remdesivir (MedChemExpress; cat# HY-104077), or Molnupinavir (MedChemExpress; cat# HY-135853) at concentrations as described in the figure legends. Cells were infected with the indicated SARS-CoV-2 strains. After 24h, infection was revealed as described above. The percentage of inhibition of infection was calculated using the area of N-positive cells as a value with the following formula: 100 × (1 − (value with drugs − value in 'non-infected')/(value in 'no drugs' − value in 'non-infected')).

The monoclonal antibodies used in this study were previously described (Bruel *et al.*, 2022a; Planas *et al.*, 2023). Neutralizing activity and ED50 were measured as described in the "S-Fuse neutralization assay" section.

Plasmids

SARS-CoV-2 spikes (from D614G, Delta, BA.1, BA.4/5, BQ1.1, XBB.1.5/9, XBB.1.16, EG.5.1, BA.2.86 isolated) were human codon-optimized and produced in silico (GeneArt, Thermo Fisher Scientific) as described (Bolland *et al.*, 2023; Buchrieser *et al.*, 2020). Spike sequences were cloned into a phCMV backbone (GenBank: AJ318514) using Gateway cloning (Thermo Fisher Scientific) or restriction enzyme digestion followed by ligation with T4 DNA ligase (New England Biolabs). The pQCXIP-Empty plasmid was used as a negative control (Bolland *et al.*, 2023; Buchrieser *et al.*, 2020). All plasmids were sequenced by the Eurofins Genomics TubeSeq service. His-tagged recombinant ACE2 ectodomain (amino acids 19–615) was cloned into pcDNA3.1 vector, produced by transient transfection of HEK293-F cells, and purified by affinity chromatography. Purified ACE2 protein was biotinylated using the EZ-Link Sulfo-NHS-Biotin kit (Thermo Fisher Scientific) as reported previously (Planchais et al., 2022).

Donor Acceptor fusion assay

To assess the fusion of the respective spike constructs, syncytia formation assays were performed as described (Bolland *et al.*, 2023; Buchrieser *et al.*, 2020). Briefly, 293T-GFP-11 cells were transfected in suspension at 37°C for 30 minutes. The transfection mix was prepared using Lipofectamine 2000 (Thermo Fisher, Scientific 179) with 50 ng of DNA in a 1:10 ratio of SARS-CoV-2-S and pQCXIP-Empty, respectively, before being added to the cells. Following transfection, cells were washed and resuspended in DMEM with 10% FBS. The level of transfection was quantified by surface staining of Spike with pan-coronavirus mAb10 antibody (previously described in Planas, NatMed, 2021?) 18 h post-transfection. Subsequently, 30,000 transfected HEK293T cells were co-cultured with 15,000 IGROV-1-GFP-1-10, VeroE6-GFP1-10, or VeroE6 TMP-1 GFP-1-10 cells per well in a µClear black 96-well plate. 18 h post-transfection, Hoechst 33342 (Invitrogen, cat# H3570) was added to the media at a 1:10,000 dilution and images were acquired using the Opera Phenix High-Content Screening System (PerkinElmer). Analysis was performed using Harmony 191 High-Content Imaging and Analysis Software (PerkinElmer, HH17000012, v.5.0), including the counting of nuclei and the GFP area.

Soluble ACE2 binding

IGROV-1 cells were seeded in a 6-well plate 12 h before infection with the indicated SARS-CoV-2 variants. The viral inoculum amount was calculated to achieve 50% of infected cells (N-positive cells) at 24 h post-infection. Afterward, the cells were detached in PBS-EDTA (0.1%) and split into a 96-well plate, with 200,000 cells per well. Cells were incubated with serial dilutions concentrations of a soluble biotinylated human ACE2 (Planchais *et al.*, 2022). Cells were washed twice with PBS and stained with Streptavidin Alexa Fluor 647 (dilution 1:500, Invitrogen; cat# S32357) for 30 minutes. Cells were then washed twice with PBS and fixed using 4% PFA (Electron microscopy; cat# 15714-S). Cells were then intracellularly stained with anti-SARS-CoV-2 nucleoprotein (N) antibody NCP-1, as described above. Cells were acquired using an Attune NxT Flow Cytometer (Thermo Fisher). Data were analyzed using FlowJo software (BDBioSciences).

S-Fuse neutralization assay

U2OS-ACE2 GFP1-10 or GFP 11 cells, also termed S-Fuse cells, become GFP+ when they are productively infected by SARS-CoV-2 (Buchrieser *et al.*, 2020) (Planas et al., 2021a). Cells were mixed (ratio 1:1) and plated at 8×10^3 per well in a µClear 96-well plate (Greiner Bio-One). The indicated SARS-CoV-2 strains were incubated with serially diluted monoclonal antibodies or sera for 15 min at room temperature and added to S-Fuse cells. Sera were heat-inactivated for 30 min at 56 °C before use. 18 h later, cells were fixed with 2% PFA (Electron microscopy cat# 15714-S), washed and stained

with Hoechst (dilution of 1:1,000, Invitrogen, Invitrogen cat# H3570). Images were acquired using an Opera Phenix high-content confocal microscope (PerkinElmer). The GFP area and the number of nuclei were quantified using the Harmony software (PerkinElmer). The percentage of neutralization was calculated using the number of syncytia as value with the following formula: 100 × (1 – (value with serum – value in 'non-infected')/(value in 'no serum' – value in 'non-infected')).
Neutralizing activity of each serum was expressed as the half maximal effective dilution (ED50). ED50 values (in ng/ml for monoclonal antibodies and in dilution values – i.e titers – for sera) were calculated with a reconstructed curve using the percentage of neutralization at each concentration.

Human nasal epithelium cells (hNEC) culture, infection and imaging

MucilAirTM, reconstructed human nasal epithelial cells (hNECs) that had been differentiated for 4 weeks prior to obtention, were cultured in 700 µl MucilAirTM media on the basal side of the air/liquid interface (ALI) cultures and monitored for healthy cilia movements. One hour prior to infection, mucus was removed from the apical side of the culture by washing the apical side with warm 200 µl MucilAir™ media. Cells were then infected with equal virus titres in 100 µL MucilAir™ media for 2 hours. Viral input was removed and stored at -80°C. Cells were then washed 2 times for 10 min at 37°C in warm PBS and then 20 min in 200 µL MucilAir™ media for the day 0 recording. Washing with 100 µl of MucilAir™ warm media was repeated every 24 h for 96 h. Every wash was subsequently centrifuged at 1500 rpm to remove cell debris and frozen at -80°C. After 96 h, cells were fixed on the apical and basal sides with 4% PFA for 45 minutes. For imaging, fixed cells were stained intracellularly with anti-SARS-CoV-2 nucleoprotein (N) antibody NCP-1, anti-alpha tubulin (66031-1-Ig; Proteintech), rabbit anti-cleaved caspase-3 (D175; Cell Signaling Technology) and phalloidin-Atto 565/633 (75784-1MG-F; Sigma) and imaged using the LSM-700 confocal microscope (Zeiss) as described (Saunders *et al.*, 2023) (Bolland *et al.*, 2023).

Staining of ACE2 and TMPRSS2

Surface expression of TMPRSS2 and ACE2 was assessed on live cells by staining with anti-TMPRSS2 VHH-A01-Fc (Saunders *et al.*, 2023) at 1 µg/ml or with anti-ACE2 VHH-B07-Fc (Brelot et al, manuscript in preparation) at 0.5 µg/ml, for 30 min at 4°C in MACS buffer. Then, cells were stained with Alexa Fluor 647-conjugated goat anti-human antibody (Invitrogen; cat# A-21445, 1/500). The control VHH Fc (R3VQFc) recognizes an unrelated protein (phosphorylated Tau protein).

Phylogenetic tree inference and lineage monitoring

SARS-CoV-2 contextual sequence names were retrieved from the Nextstrain build of Sept. 18 2023 (Hadfield et al., 2018). All available SARS-CoV-2 sequences from human infections were

downloaded from the GISAID Epicov database (https://gisaid.org/) on October 23, 2023, and only sequences longer than 29000 nucleotides and with less than 1% ambiguities (Ns) were kept. Sequences were reannotated using pangolin (v4.3.1, with option --usher), and aligned against the Wuhan-Hu1 reference sequence (GenBank MN908947) using nextalign v2.14.0. In addition to this global context, BA.2.86 sequences were added to the dataset, using gofasta v1.2.1 (Jackson, 2022). The alignment used for phylogenetic reconstruction was made of 2909 sequences (global context sequences with the addition of BA.2.86 sequences and their closest relatives). Specific positions of the alignment were masked using goalign v0.3.5 (goalign mask command) to decrease phylogenetic noise. Bootstrap alignments were generated using goalign v0.3.5 (goalign build seqboot command) and reference and bootstrap trees were inferred using iqtree v2.2.0 (iqtree -m GTR -ninit 2 -n 2 -me 0.05 -nt AUTO -ninit 10 -n 4). Bootstrap supports were computed using gotree v0.4.4 (gotree compute support fbp).

Mutations that are common and specific to lineages of interest were computed using the outbreak.info R package (https://outbreak-info.github.io/R-outbreak-info) on Oct. 23rd 2023. Values for some insertions or deletions were manually computed. Hierarchical relationships between lineages were retrieved from the pangolin GitHub repository (https://github.com/cov-lineages/pango-designation).

The evolution of the prevalence of SARS-CoV-2 lineages throughout 2023 was visualized using R 4.3 and ggplot 3.4.3, using GISAID data from January 1st, 2023 to October 7th, 2023. Data and workflows used to generate the figures are publicly available at https://github.com/SimonLoriereLab/sarscov2_Oct2023.

All genome sequences and associated metadata used to build Fig. 1 and S1 are published in GISAID's EpiCoV database. To view the contributors of each individual sequence with details such as accession number, Virus name, Collection date, Originating Lab and Submitting Lab and the list of Authors, visit https://doi.org/10.55876/gis8.231102ka (Fig. 1a) or https://doi.org/10.55876/gis8.231020kn (Fig. 1b).

Statistical analysis

Flow cytometry data were analysed using FlowJo v.10 (TriStar). Calculations were performed using Excel 365 (Microsoft). Figures were generated using Prism 9 (GraphPad Software). Statistical analysis was conducted using GraphPad Prism 9. Statistical significance between different groups was calculated using the tests indicated in each figure legend.

Data availability

All data supporting the findings of this study are available within the article or from the corresponding authors upon reasonable request without any restrictions. The raw data generated in this study are

provided in the Source Data file. The sequencing data generated in this study have been deposited in the GISAID EpiCoV database (EPI_SET ID: EPI_SET_231113yq).

Figure Legends.

Figure 1. SARS-CoV2 evolution in 2023 and Spike mutation patterns of the main SARS-CoV-2 lineages. a. Evolution of the prevalence of main SARS-CoV-2 lineages from January to October 2023. The pattern of emergence and replacement of several lineages, such as XBB.1.5, then XBB.1.9, XBB.1.16 or EG.5.1 is shown. The variants with a frame are analyzed in this study. **b.** Changes specific to lineages studied here in comparison to Omicron BA.2 are displayed as colored squares. The spike domain organization is displayed on the top, with N-terminal domain (NTD), Receptor Binding Domain (RBD), Receptor Binding Motif (RBM), Single domains SD1 and SD2, the S1/S2 cleavage site, and S2 domains. BA.2.86 shows many new mutations compared to other lineages. A complete comparison of spike mutations compared to the reference Wuhan_Hu-1 is presented in Fig S1b.

Figure 2. Replication kinetics of SARS-CoV-2 variants in Vero E6, Vero E6 TMP-1 and -2 and IGROV-1 cells. a. Cells were infected with the indicated variants, at $3x10^{-2}$ virus per cells. Cells were stained with a pan-coronavirus anti-N antibody at days 1 to 4 pi. The N-positive areas were plotted on the graph. Each curve represents an independent experiment. **b.** Comparison of the effect of E-64d and SB412515 against different variants. IGROV-1 cells were pre-incubated 2 h with serial dilutions of E-64d or SB412515 (30 to $1.7x10^{-4}$ µM) and infected with D614G, XBB.1.5.1, EG.5.1.3, or BA.2.86.1. The percentage of inhibition is represented. Data are mean ± s.d. of 3 independent experiments.

Figure 3. Fusogenicity and binding to ACE2 of the variant Spike proteins. a. Schematic representation of the coculture system. 293T GFP-11 donor cells were transfected with the indicated variant Spike expression plasmids and cocultivated with IGROV-1, Vero E6 or Vero E6 TMP-1 acceptor cells expressing GFP1-10. The area of GFP+ fused cells was measured after 18 h. **b.** Representative images of cell-cell fusion between 293T donor cells and IGROV-1 acceptor cells. Scale bar, 200 µm. **c.** Fusogenicity of the different spikes with IGROV-1 acceptor cells. Each dot represents a single experiment. Data are mean ± s.d. of 4-6 independent experiments. One-way ANOVA with Kruskal-Wallis test followed by Dunn's test for multiple comparisons to compare Delta with respective variants were conducted. **d.** Effect of TMPRSS2 on the fusion of the different Spikes. Cell-cell fusion assays were performed with Vero E6 or Vero E6 TMP-1 as target cells. Data are mean ± s.d. of 4 independent experiments. Paired t-test to compare fusion in Vero E6 versus Vero E6 TMP-1 were conducted. **e,f.**

Binding of soluble ACE2 to IGROV-1 infected cells (e) or to 293T cells transiently expressing the Spike (f). Cells were stained with a soluble form of ACE2 (hACE2-Fc) with a serial dilution of hACE2-Fc. EC50 of soluble ACE2 (µg/ml) for different variant Spikes proteins. Data are mean ± s.d. of 3-4 independent experiments. One-way ANOVA with Kruskal-Wallis test followed by Dunn's test for multiple comparisons to compare Delta with respective variants were conducted.

Figure 4. Replication of SARS-CoV-2 variants in hNECs. Primary human nasal epithelial cells (hNECs) cultivated at the air-liquid interface (ALI) were exposed to the indicated SARS-CoV-2 variants. **a.** Viral RNA release from the apical side of hNECs was measured by RT-qPCR every 24 h up to 96 h pi. Replication kinetics of each variant from one representative experiment are represented. **b.** Comparison of viral RNA release at 24 h pi with the indicated variants. **c.** Infectious viral titers in supernatants from the apical side were quantified with S-Fuse cells at 48 h p.i. **b,c.** Data are mean ± s.d. of 4-6 independent experiments. One-way ANOVA with Kruskal-Wallis test followed by Dunn's test for multiple comparisons to compare Delta with respective variants were conducted. **d.** Immunofluorescence of hNECs stained for tubulin (cyan), actin (yellow), SARS-CoV-2 Nucleocapsid (green) and cleavedcaspase-3 (red). Shown is one representative field (150x150 mm) of each variant. Scale bar = 20 µm.

Figure 5. Activity of neutralizing mAbs and antiviral drugs against SARS-CoV-2 variants. a. Neutralization curves of previously approved mAbs. Dose–response analysis of neutralization of the indicated variants by Sotrovimab, Evusheld (Cilgavimab and Tixagevima) and Ronapreve (Casirivimab and Imdevimab). **b.** Inhibitory curves of antiviral drugs against the indicated variants. Dose-response analysis of the antiviral effect of Nirmatrelvir, Remdesivir and Molnupiravir. **a,b.** Data are mean ± s.d. of 3 independent experiments.

Figure 6. Sensitivity of SARS-CoV-2 variants to sera of vaccinated and/or infected individuals. Neutralization titers of the sera against the indicated viral variants are expressed as ED50. **a.** Neutralizing activity of sera from individuals vaccinated with 3 doses of Pfizer vaccine. Sera (n= 21) were sampled 25 – 475 days after the third dose. 15/21 had a breakthrough infection at the time of BA.1/2 circulation. **b,c.** Neutralizing activity of sera from individuals having received the bivalent Wuhan/BA.5 Pfizer boost. Sera were sampled one month (b; n= 20) and six months (c; n=14) after the booster dose. **d.** Temporal evolution of Neutralizing Antibody (Nab) titers against D614G, BA.5, EG.5.1.3 and BA.2.86.1 after bivalent Wuhan/BA.5 booster dose. The Nab titers were calculated at the time of injection (month 0) and at the indicated months after injection. **e.** Neutralizing activity of sera from Pfizer-vaccinated recipients after XBB-derived breakthrough infections (infections occurred in

September 2023, when XBB-derived variants were predominantly circulating in France). Sera were sampled 10 to 50 days after the breakthrough (n=12). The dotted line indicates the limit of detection (ED50 = 30). Each dot represents the mean of n=2 independent experiments. Black lines represent the median values. Two-sided Friedman test with Dunn's test for multiple comparisons was performed to compare each viral strain to D614G.

Figure S1. Maximum likelihood phylogeny representing the evolution of the main lineages of SARS-CoV-2 since the beginning of the epidemic. **a.** The red circle indicates one of the first sequences (Wuhan/Hu-1/2019). The BA.2.86 sequences are located inside the BA.2 clade, at the end of a long branch. Of note, a limitation of the inferred phylogeny is that known recombinant lineages (e.g. XBF or XBB) were included in the dataset, and their branching should be interpreted with caution. **b.** Comparison of spike mutations compared to the reference Wuhan_Hu-1 for selected SARS-CoV-2 variants.

Figure S2: ACE2 and TMPRSS2 expression in cell lines. IGROV-1, Vero E6, Vero E6 TMP-1 and TMP-2 cells were stained with anti-ACE2 or anti-TMPRSS2 antibodies and analyzed by flow cytometry. Representative examples of the gating strategy in IGROV-1 cells and of the signals obtained in cell lines are shown.

Figure S3. Permissibility of IGROV-1 and Vero E6 cells to SARS-CoV-2 variants. Viral titrations in IGROV-1 and Vero E6 cells. Cells were infected with serial dilutions of the indicated variants. At 24 hours post-infection (p.i.), cells were stained with a pan-coronavirus anti-N antibody (green) and Hoechst to visualize the nuclei (blue). **a.** The N positive areas in IGROV-1 (blue curves) and Vero E6 cells (grey curves) were compared for each viral dilution. The dotted line corresponds to the signal obtained with the first dilution (1/20) in IGROV-1 cells, set to the arbitrary value of 1. Data are mean ± s.d. of 3-5 independent experiments. **b.** Representative images with the indicated viral strains. An identical viral inoculum was used in the two cell lines. Scale bar, 200 µm.

Figure S4. Effect of the TMPRSS2 inhibitor Camostat and Cathepsin L inhibitors E-64d and SB412515 on viral infection a. IGROV-1, Vero E6 and Vero E6 TMP-1 cells pre-incubated 2 h with Camostat (100 µM), E-64d (10 µM), or SB412515 (10 µM) and exposed to the D614G, Delta, BA.1, XBB.1, or XBB.1.16.1 variants for 24 h. The viral inoculum was determined by titration in each cell line to achieve a similar N-positive area at 24 h pi. The cells were stained with a pan-coronavirus anti-N antibody. Hoechst was used to visualize the nuclei for evaluating drug toxicity. The percentage of infection compared to the

control (without drugs, represented by the dotted line) is shown. Data are mean ± s.d. of 3 independent experiments.

Figure S5. Spike expression in 293T cells. Gating strategy and levels of Spike at the cell surface. 293T cells transiently expressing the indicated variant Spikes were stained with a pan-coronavirus anti-S2 mAb 18 h post-transfection and analyzed by flow cytometry.

Figure S6. Binding of variant Spike proteins to ACE2. The affinity of the variant Spike proteins expressed at the surface of IGROV-1 infected cells was assessed by staining the cells and flow cytometry analysis. IGROV-1 cells were infected with the indicated variants. **a.** Representative examples of the gating strategy. **b.** The percentages of hACE2-Fc+ cells are represented at various dilutions of hACE2-Fc. Data are mean ± s.d. of 3-4 independent experiments.

Figure S7. Sotrobimab binding to infected cells. IGROV-1 cells were infected with the indicated virus for 24h. Then, cells were stained with Sotrovimab or the pan-coronavirus anti-S2 mAb10 antibody. After fixation, cells were intracellularly stained with anti-SARS-CoV-2 nucleoprotein (N) antibody NCP-1 and analyzed by flow cytometry. Representative examples of the gating strategy **(a)** and co-staining of Nucleocapsid and Sotrovimab **(b)** or mAb10 **(c).**

Acknowledgements

The authors thank the patients who participated to this study, members of the Virus and Immunity Unit and other teams for discussion and help, Julien Puech from Hôpital Europeen Georges Pompidou for organizing the collect and analysis of nasopharyngeal swabs, Hugo Mouquet and Cyril Planchais for the kind gift of reagents, Nathalie Aulner and the staff at the UtechS Photonic BioImaging (UPBI) core facility (Institut Pasteur), a member of the France BioImaging network, for image acquisition and analysis, , Fabienne Peira, Vanessa Legros, Aurelie Theillay, Sandra Pallay and Daniela Pires Roteia (CHU Orléans) for their help with the cohorts. The authors thank "the Centre de Ressources biologiques" from Hospices Civils de Lyon (BRIF number: BB-0033-00046), the members of the National Reference Center for viruses of respiratory infections hosted at Institut Pasteur, and the Mutualized platform for Microbiology (P2M). This work has used the computational and storage services (Maestro cluster) provided by the IT department at Institut Pasteur, Paris

Funding

Work in OS lab is funded by Institut Pasteur, Urgence COVID-19 Fundraising Campaign of Institut Pasteur, Fondation pour la Recherche Médicale (FRM), ANRS, the Vaccine Research Institute (ANR-10-LABX-77), Labex IBEID (ANR-10-LABX-62-IBEID), ANR / FRM Flash Covid PROTEO-SARS-CoV-2, ANR Coronamito, HERA european funding, Sanofi and IDISCOVR. DP is supported by the Vaccine Research Institute. The E.S.-L. laboratory is funded by Institut Pasteur, the INCEPTION program (Investissements d'Avenir grant ANR-16-CONV-0005), the Ixcore foundation for research, the French Government's Investissement d'Avenir programme, Laboratoire d'Excellence 'Integrative Biology of Emerging Infectious Diseases' (grant no. ANR-10-LABX-62-IBEID), the HERA Project DURABLE (grant no 101102733) and the NIH PICREID (grant no U01AI151758). The Opera system was co-funded by Institut Pasteur and the Région ile de France (DIM1Health). Work in UPBI is funded by grant ANR-10-INSB-04-01 and Région Ile-de-France program DIM1-Health. The funders of this study had no role in study design, data collection, analysis and interpretation, or writing of the article.

Author Contributions Statement

Experimental strategy design, experiments: D.P., I.S., F.P., F.G-B, W.B., M.H., J.B., T.V., O.S.
Vital materials: F.D., P.R., D.V., H.P., B.L., S.T-A. L.H., T.P., E.S-L.
Phylogenetic analysis: F.L., E.S-L.
Viral sequencing: M.P., D.V., H.P., B.L., E.S-L.
Manuscript writing and editing: D.P., E.S-L., O.S.

Competing Interests Statement

The authors declare no competing interests.

References

Abu-Raddad, L.J., Chemaitelly, H., Ayoub, H.H., AlMukdad, S., Yassine, H.M., Al-Khatib, H.A., Smatti, M.K., Tang, P., Hasan, M.R., Coyle, P., et al. (2022). Effect of mRNA Vaccine Boosters against SARS-CoV-2 Omicron Infection in Qatar. New England Journal of Medicine *386*, 1804-1816. 10.1056/NEJMoa2200797.

Addetia, A., Piccoli, L., Case, J.B., Park, Y.-J., Beltramello, M., Guarino, B., Dang, H., de Melo, G.D., Pinto, D., Sprouse, K., et al. (2023). Neutralization, effector function and immune imprinting of Omicron variants. Nature *621*, 592-601. 10.1038/s41586-023-06487-6.

Aggarwal, A., Fichter, C., Milogiannakis, V., Akerman, A., Ison, T., Silva, M.R., Esneau, C., Bartlett, N., Burrell, L., Patel, S., et al. (2023). TMPRSS2 activation of Omicron lineage Spike glycoproteins is regulated by TMPRSS2 cleavage of ACE2. Biorxiv, 2023.2009.2022.558930. 10.1101/2023.09.22.558930.

Andrews, N., Stowe, J., Kirsebom, F., Toffa, S., Rickeard, T., Gallagher, E., Gower, C., Kall, M., Groves, N., O'Connell, A.-M., et al. (2022). Covid-19 Vaccine Effectiveness against the Omicron (B.1.1.529) Variant. New England Journal of Medicine *386*, 1532-1546. 10.1056/NEJMoa2119451.

Barnes, C.O., Jette, C.A., Abernathy, M.E., Dam, K.-M.A., Esswein, S.R., Gristick, H.B., Malyutin, A.G., Sharaf, N.G., Huey-Tubman, K.E., Lee, Y.E., et al. (2020). SARS-CoV-2 neutralizing antibody structures inform therapeutic strategies. Nature *588*, 682-687. 10.1038/s41586-020-2852-1 PMID - 33045718.
Bolland, W., Michel, V., Planas, D., Hubert, M., Guivel-Benhassine, F., Porrot, F., Staropoli, I., N'Debi, M., Rodriguez, C., Fourati, S., et al. (2023). High fusion and cytopathy of SARS-CoV-2 variant B.1.640.1. Biorxiv, 2023.2009.2006.556548. 10.1101/2023.09.06.556548.
Bouhaddou, M., Reuschl, A.-K., Polacco, B.J., Thorne, L.G., Ummadi, M.R., Ye, C., Rosales, R., Pelin, A., Batra, J., Jang, G.M., et al. (2023). SARS-CoV-2 variants evolve convergent strategies to remodel the host response. Cell *186*, 4597-4614.e4526. 10.1016/j.cell.2023.08.026.
Bruel, T., Hadjadj, J., Maes, P., Planas, D., Seve, A., Staropoli, I., Guivel-Benhassine, F., Porrot, F., Bolland, W.-H., Nguyen, Y., et al. (2022a). Serum neutralization of SARS-CoV-2 Omicron sublineages BA.1 and BA.2 in patients receiving monoclonal antibodies. Nature Medicine *28*, 1297-1302. 10.1038/s41591-022-01792-5 PMID - 35322239.
Bruel, T., Stéfic, K., Nguyen, Y., Toniutti, D., Staropoli, I., Porrot, F., Guivel-Benhassine, F., Bolland, W.-H., Planas, D., Hadjadj, J., et al. (2022b). Longitudinal analysis of serum neutralization of SARS-CoV-2 Omicron BA.2, BA.4, and BA.5 in patients receiving monoclonal antibodies. Cell Reports Medicine, 100850. https://doi.org/10.1016/j.xcrm.2022.100850.
Bruel, T., Vrignaud, L.-L., Porrot, F., Staropoli, I., Planas, D., Guivel-Benhassine, F., Puech, J., Prot, M., Munier, S., Bolland, W.H., et al. (2023). Sotrovimab therapy elicits antiviral activities against Omicron BQ.1.1 and XBB.1.5 in sera of immunocompromised patients. Med *4*, 664-667. https://doi.org/10.1016/j.medj.2023.07.007.
Buchrieser, J., Dufloo, J., Hubert, M., Monel, B., Planas, D., Rajah, M.M., Planchais, C., Porrot, F., Guivel-Benhassine, F., Van der Werf, S., et al. (2020). Syncytia formation by SARS-CoV-2-infected cells. EMBO J *39*, e106267. 10.15252/embj.2020106267.
Cao, Y., Jian, F., Wang, J., Yu, Y., Song, W., Yisimayi, A., Wang, J., An, R., Chen, X., Zhang, N., et al. (2022a). Imprinted SARS-CoV-2 humoral immunity induces convergent Omicron RBD evolution. Nature, https://doi.org/10.1038/s41586-41022-05644-41587. 10.1038/s41586-022-05644-7.
Cao, Y., Song, W., Wang, L., Liu, P., Yue, C., Jian, F., Yu, Y., Yisimayi, A., Wang, P., Wang, Y., et al. (2022b). Characterization of the enhanced infectivity and antibody evasion of Omicron BA.2.75. Cell Host & Microbe *30*, 1527-1539.e1525. https://doi.org/10.1016/j.chom.2022.09.018.
Chalkias, S., McGhee, N., Whatley, J.L., Essink, B., Brosz, A., Tomassini, J.E., Girard, B., Wu, K., Edwards, D.K., Nasir, A., et al. (2023). Safety and Immunogenicity of XBB.1.5-Containing mRNA Vaccines. medRxiv, 2023.2008.2022.23293434. 10.1101/2023.08.22.23293434.
Crotty, S. (2021). Hybrid immunity. Science *372*, 1392-1393. doi:10.1126/science.abj2258.
Faraone, J.N., Qu, P., Goodarzi, N., Zheng, Y.-M., Carlin, C., Saif, L.J., Oltz, E.M., Xu, K., Jones, D., Gumina, R.J., and Liu, S.-L. (2023). Immune Evasion and Membrane Fusion of SARS-CoV-2 XBB Subvariants EG.5.1 and XBB.2.3. Biorxiv, 2023.2008.2030.555188. 10.1101/2023.08.30.555188.
France, S.p. (2022). Point épidémiologique COVID-19 du 10 février 2022. . https://www.santepubliquefrance.fr/presse/2022/point-epidemiologique-covid-19-du-10-fevrier-2022-le-ralentissement-de-la-circulation-du-sars-cov-2-se-confirme-et-s-accompagne-d-une-baisse-des.

Gruell, H., Vanshylla, K., Weber, T., Barnes, C.O., Kreer, C., and Klein, F. (2022). Antibody-mediated neutralization of SARS-CoV-2. Immunity *55*, 925-944. https://doi.org/10.1016/j.immuni.2022.05.005.
Hadfield, J., Megill, C., Bell, S.M., Huddleston, J., Potter, B., Callender, C., Sagulenko, P., Bedford, T., and Neher, R.A. (2018). Nextstrain: real-time tracking of pathogen evolution. Bioinformatics *34*, 4121-4123. 10.1093/bioinformatics/bty407.
Herder, V., Mendonca, D.C., Upfold, N., Furnon, W., Kerr, K., Ilia, G., Allan, J., Sigal, A., Patel, A.H., and Palmarini, M. (2023). The SARS-CoV-2 Omicron sub-variant BA.2.86 is attenuated in hamsters. Biorxiv, 2023.2011.2010.566576. 10.1101/2023.11.10.566576.
Heurich, A., Hofmann-Winkler, H., Gierer, S., Liepold, T., Jahn, O., and Pöhlmann, S. (2014). TMPRSS2 and ADAM17 Cleave ACE2 Differentially and Only Proteolysis by TMPRSS2 Augments Entry Driven by the Severe Acute Respiratory Syndrome Coronavirus Spike Protein. Journal of Virology *88*, 1293-1307. 10.1128/jvi.02202-13.
Hu, Y., Zou, J., Kurhade, C., Deng, X., Chang, H.C., Kim, D.K., Shi, P.-Y., Ren, P., and Xie, X. (2023). Less neutralization evasion of SARS-CoV-2 BA.2.86 than XBB sublineages and CH.1.1. Biorxiv, 2023.2009.2010.557047. 10.1101/2023.09.10.557047.
Jackson, B. (2022). gofasta: command-line utilities for genomic epidemiology research. Bioinformatics *38*, 4033-4035. 10.1093/bioinformatics/btac424.
Khan, K., Lustig, G., Reedoy, K., Jule, Z., Römer, C., Karim, F., Ganga, Y., Bernstein, M., Baig, Z., Mahlangu, B., et al. (2023). Evolution and neutralization escape of the SARS-CoV-2 BA.2.86 subvariant. medRxiv, 2023.2009.2008.23295250. 10.1101/2023.09.08.23295250.
Koch, J., Uckeley, Z.M., Doldan, P., Stanifer, M., Boulant, S., and Lozach, P.-Y. (2021). TMPRSS2 expression dictates the entry route used by SARS-CoV-2 to infect host cells. The EMBO Journal *40*, e107821. https://doi.org/10.15252/embj.2021107821.
Krammer, F., and Ellebedy, A.H. (2023). Variant-adapted COVID-19 booster vaccines. Science *382*, 157-159. doi:10.1126/science.adh2712.
Kuhlmann, C., Mayer, C.K., Claassen, M., Maponga, T., Burgers, W.A., Keeton, R., Riou, C., Sutherland, A.D., Suliman, T., Shaw, M.L., and Preiser, W. (2022). Breakthrough infections with SARS-CoV-2 omicron despite mRNA vaccine booster dose. The Lancet *399*, 625-626. 10.1016/S0140-6736(22)00090-3.
Lasrado, N., Collier, A.-r.Y., Hachmann, N.P., Miller, J., Rowe, M., Schonberg, E.D., Rodrigues, S.L., LaPiana, A., Patio, R.C., Anand, T., et al. (2023). Neutralization Escape by SARS-CoV-2 Omicron Subvariant BA.2.86. Biorxiv, 2023.2009.2004.556272. 10.1101/2023.09.04.556272.
Lassauniere, R., Polacek, C., Baig, S., Ellegaard, K., Escobar-Herrera, L.A., Fomsgaard, A., Spiess, K., Schwartz, O., Planas, D., Simon-Loriere, E., et al. (2023). Neutralisation of SARS-CoV-2 Omicron subvariants BA.2.86 and EG.5.1 by antibodies induced by earlier infection or vaccination. Biorxiv, 2023.2010.2001.560365. 10.1101/2023.10.01.560365.
Lin, D.-Y., Xu, Y., Gu, Y., Zeng, D., Sunny, S.K., and Moore, Z. (2023). Durability of Bivalent Boosters against Omicron Subvariants. New England Journal of Medicine. 10.1056/NEJMc2302462.
Matsuyama, S., Nao, N., Shirato, K., Kawase, M., Saito, S., Takayama, I., Nagata, N., Sekizuka, T., Katoh, H., Kato, F., et al. (2020). Enhanced isolation of SARS-CoV-2 by TMPRSS2-expressing cells. Proceedings of the National Academy of Sciences *117*, 7001-7003. doi:10.1073/pnas.2002589117.
Meng, B., Abdullahi, A., Ferreira, I.A.T.M., Goonawardane, N., Saito, A., Kimura, I., Yamasoba, D., Gerber, P.P., Fatihi, S., Rathore, S., et al. (2022). Altered TMPRSS2 usage by SARS-CoV-2

Omicron impacts infectivity and fusogenicity. Nature *603*, 706-714. 10.1038/s41586-022-04474-x.
Miller, J., Hachmann, N.P., Collier, A.-r.Y., Lasrado, N., Mazurek, C.R., Patio, R.C., Powers, O., Surve, N., Theiler, J., Korber, B., and Barouch, D.H. (2023). Substantial Neutralization Escape by SARS-CoV-2 Omicron Variants BQ.1.1 and XBB.1. New England Journal of Medicine. 10.1056/NEJMc2214314.
Mlcochova, P., Kemp, S.A., Dhar, M.S., Papa, G., Meng, B., Ferreira, I.A.T.M., Datir, R., Collier, D.A., Albecka, A., Singh, S., et al. (2021). SARS-CoV-2 B.1.617.2 Delta variant replication and immune evasion. Nature *599*, 114-119. 10.1038/s41586-021-03944-y.
Moriyama, S., Anraku, Y., Taminishi, S., Adachi, Y., Kuroda, D., Kita, S., Higuchi, Y., Kirita, Y., Kotaki, R., Tonouchi, K., et al. (2023). Structural delineation and computational design of SARS-CoV-2-neutralizing antibodies against Omicron subvariants. Nature Communications *14*, 4198. 10.1038/s41467-023-39890-8.
Mykytyn, A.Z., Breugem, T.I., Geurts, M.H., Beumer, J., Schipper, D., Acker, R.v., Doel, P.B.v.d., Royen, M.E.v., Zhang, J., Clevers, H., et al. (2023). SARS-CoV-2 Omicron entry is type II transmembrane serine protease-mediated in human airway and intestinal organoid models. Journal of Virology *97*, e00851-00823. doi:10.1128/jvi.00851-23.
Park, Y.-J., Pinto, D., Walls, A.C., Liu, Z., De Marco, A., Benigni, F., Zatta, F., Silacci-Fregni, C., Bassi, J., Sprouse, K.R., et al. (2022a). Imprinted antibody responses against SARS-CoV-2 Omicron sublineages. Science *378*, 619-627. doi:10.1126/science.adc9127.
Park, Y.-J., Pinto, D., Walls, A.C., Liu, Z., De Marco, A., Benigni, F., Zatta, F., Silacci-Fregni, C., Bassi, J., Sprouse, K.R., et al. (2022b). Imprinted antibody responses against SARS-CoV-2 Omicron sublineages. Science *0*, eadc9127. doi:10.1126/science.adc9127.
Planas, D., Bruel, T., Grzelak, L., Guivel-Benhassine, F., Staropoli, I., Porrot, F., Planchais, C., Buchrieser, J., Rajah, M.M., Bishop, E., et al. (2021a). Sensitivity of infectious SARS-CoV-2 B.1.1.7 and B.1.351 variants to neutralizing antibodies. Nature Medicine. 10.1038/s41591-021-01318-5.
Planas, D., Bruel, T., Staropoli, I., Guivel-Benhassine, F., Porrot, F., Maes, P., Grzelak, L., Prot, M., Mougari, S., Planchais, C., et al. (2023). Resistance of Omicron subvariants BA.2.75.2, BA.4.6, and BQ.1.1 to neutralizing antibodies. Nature Communications *14*, 824. 10.1038/s41467-023-36561-6.
Planas, D., Saunders, N., Maes, P., Guivel-Benhassine, F., Planchais, C., Buchrieser, J., Bolland, W.H., Porrot, F., Staropoli, I., Lemoine, F., et al. (2022a). Considerable escape of SARS-CoV-2 Omicron to antibody neutralization. Nature *602*, 671-675. 10.1038/s41586-021-04389-z.
Planas, D., Staropoli, I., Porot, F., Guivel-Benhassine, F., Handala, L., Prot, M., Bolland, W.-H., Puech, J., Péré, H., Veyer, D., et al. (2022b). Duration of BA.5 neutralization in sera and nasal swabs from SARS-CoV-2 vaccinated individuals, with or without omicron breakthrough infection. Med *3*, 838-847.e833. https://doi.org/10.1016/j.medj.2022.09.010.
Planas, D., Veyer, D., Baidaliuk, A., Staropoli, I., Guivel-Benhassine, F., Rajah, M.M., Planchais, C., Porrot, F., Robillard, N., Puech, J., et al. (2021b). Reduced sensitivity of SARS-CoV-2 variant Delta to antibody neutralization. Nature *596*, 276-280. 10.1038/s41586-021-03777-9.
Planchais, C., Fernández, I., Bruel, T., de Melo, G.D., Prot, M., Beretta, M., Guardado-Calvo, P., Dufloo, J., Molinos-Albert, L.M., Backovic, M., et al. (2022). Potent human broadly SARS-CoV-2–neutralizing IgA and IgG antibodies effective against Omicron BA.1 and BA.2. Journal of Experimental Medicine *219*. 10.1084/jem.20220638.
Pulliam, J.R.C., van Schalkwyk, C., Govender, N., von Gottberg, A., Cohen, C., Groome, M.J., Dushoff, J., Mlisana, K., and Moultrie, H. (2022). Increased risk of SARS-CoV-2 reinfection

associated with emergence of Omicron in South Africa. Science *376*, eabn4947. doi:10.1126/science.abn4947.
Qu, P., Xu, K., Faraone, J.N., Goodarzi, N., Zheng, Y.-M., Carlin, C., Bednash, J.S., Horowitz, J.C., Mallampalli, R.K., Saif, L.J., et al. (2023). Immune Evasion, Infectivity, and Fusogenicity of SARS-CoV-2 Omicron BA.2.86 and FLip Variants. Biorxiv, 2023.2009.2011.557206. 10.1101/2023.09.11.557206.
Ragonnet-Cronin, M., Nutalai, R., Huo, J., Dijokaite-Guraliuc, A., Das, R., Tuekprakhon, A., Supasa, P., Liu, C., Selvaraj, M., Groves, N., et al. (2023). Generation of SARS-CoV-2 escape mutations by monoclonal antibody therapy. Nature Communications *14*, 3334. 10.1038/s41467-023-37826-w.
Rajah, M.M., Hubert, M., Bishop, E., Saunders, N., Robinot, R., Grzelak, L., Planas, D., Dufloo, J., Gellenoncourt, S., Bongers, A., et al. (2021). SARS-CoV-2 Alpha, Beta, and Delta variants display enhanced Spike-mediated syncytia formation. The EMBO Journal *n/a*, e108944. https://doi.org/10.15252/embj.2021108944.
Reeve, L., Tessier, E., Trindall, A., Abdul Aziz, N.I.B., Andrews, N., Futschik, M., Rayner, J., Didier'Serre, A., Hams, R., Groves, N., et al. (2023). High attack rate in a large care home outbreak of SARS-CoV-2 BA.2.86, East of England, August 2023. Eurosurveillance *28*, 2300489. doi:https://doi.org/10.2807/1560-7917.ES.2023.28.39.2300489.
Robinot, R., Hubert, M., de Melo, G.D., Lazarini, F., Bruel, T., Smith, N., Levallois, S., Larrous, F., Fernandes, J., Gellenoncourt, S., et al. (2021). SARS-CoV-2 infection induces the dedifferentiation of multiciliated cells and impairs mucociliary clearance. Nature Communications *12*, 4354. 10.1038/s41467-021-24521-x.
Saunders, N., Fernandez, I., Planchais, C., Michel, V., Rajah, M.M., Baquero Salazar, E., Postal, J., Porrot, F., Guivel-Benhassine, F., Blanc, C., et al. (2023). TMPRSS2 is a functional receptor for human coronavirus HKU1. Nature. 10.1038/s41586-023-06761-7.
Sheward, D.J., Yang, Y., Westerberg, M., Öling, S., Muschiol, S., Sato, K., Peacock, T.P., Hedestam, G.B.K., Albert, J., and Murrell, B. (2023). Sensitivity of BA.2.86 to prevailing neutralising antibody responses. Biorxiv, 2023.2009.2002.556033. 10.1101/2023.09.02.556033.
Suzuki, R., Yamasoba, D., Kimura, I., Wang, L., Kishimoto, M., Ito, J., Morioka, Y., Nao, N., Nasser, H., Uriu, K., et al. (2022). Attenuated fusogenicity and pathogenicity of SARS-CoV-2 Omicron variant. Nature *603*, 700-705. 10.1038/s41586-022-04462-1.
Tamura, T., Mizuma, K., Nasser, H., Deguchi, S., Padilla-Blanco, M., Uriu, K., Tolentino, J.E.M., Tsujino, S., Suzuki, R., Kojima, I., et al. (2023). Virological characteristics of the SARS-CoV-2 BA.2.86 variant. Biorxiv, 2023.2011.2002.565304. 10.1101/2023.11.02.565304.
Tegally, H., Moir, M., Everatt, J., Giovanetti, M., Scheepers, C., Wilkinson, E., Subramoney, K., Makatini, Z., Moyo, S., Amoako, D.G., et al. (2022). Emergence of SARS-CoV-2 Omicron lineages BA.4 and BA.5 in South Africa. Nature Medicine *28*, 1785-1790. 10.1038/s41591-022-01911-2.
Trouillet-Assant, S., Vega, C.A., Bal, A., Nazare, J.A., Fascia, P., Paul, A., Massardier-Pilonchery, A., Aubarede, C.d., Guibert, N., Pitiot, V., et al. (2020). Assessment of serological techniques for screening patients for COVID-19 (COVID-SER): a prospective, multicentric study. BMJ Open *10*, e041268. 10.1136/bmjopen-2020-041268.
Uraki, R., Kiso, M., Iwatsuki-Horimoto, K., Yamayoshi, S., Ito, M., Chiba, S., Sakai-Tagawa, Y., Imai, M., Kashima, Y., Koga, M., et al. (2023). Characterization of an EG.5.1 clinical isolate in vitro and in vivo. Biorxiv, 2023.2008.2031.555819. 10.1101/2023.08.31.555819.

Uriu, K., Ito, J., Kosugi, Y., Tanaka, Y.L., Mugita, Y., Guo, Z., Hinay, A.A., Putri, O., Kim, Y., Shimizu, R., et al. (2023). Transmissibility, infectivity, and immune evasion of the SARS-CoV-2 BA.2.86 variant. The Lancet Infectious Diseases. https://doi.org/10.1016/S1473-3099(23)00575-3.

Viana, R., Moyo, S., Amoako, D.G., Tegally, H., Scheepers, C., Althaus, C.L., Anyaneji, U.J., Bester, P.A., Boni, M.F., Chand, M., et al. (2022). Rapid epidemic expansion of the SARS-CoV-2 Omicron variant in southern Africa. Nature *603*, 679-686. 10.1038/s41586-022-04411-y.

Wang, Q., Guo, Y., Liu, L., Schwanz, L.T., Li, Z., Nair, M.S., Ho, J., Zhang, R.M., Iketani, S., Yu, J., et al. (2023a). Antigenicity and receptor affinity of SARS-CoV-2 BA.2.86 spike. Nature. 10.1038/s41586-023-06750-w.

Wang, Q., Guo, Y., Zhang, R.M., Ho, J., Mohri, H., Valdez, R., Manthei, D.M., Gordon, A., Liu, L., and Ho, D.D. (2023b). Antibody Neutralization of Emerging SARS-CoV-2: EG.5.1 and XBC.1.6. Biorxiv, 2023.2008.2021.553968. 10.1101/2023.08.21.553968.

Wang, Q., Iketani, S., Li, Z., Liu, L., Guo, Y., Huang, Y., Bowen, A.D., Liu, M., Wang, M., Yu, J., et al. (2022). Alarming antibody evasion properties of rising SARS-CoV-2 BQ and XBB subvariants. Cell. 10.1016/j.cell.2022.12.018.

WHO (2022). Therapeutics and COVID-19: living guideline. Sept 16, 2022 Update https://www.who. int/publications/i/item/WHO-2019-nCoV- therapeutics-2022.5.

WHO (2023). Tracking SARS-CoV-2 variants. https://www.who.int/activities/tracking-SARS-CoV-2-variants.

Willett, B.J., Grove, J., MacLean, O.A., Wilkie, C., De Lorenzo, G., Furnon, W., Cantoni, D., Scott, S., Logan, N., Ashraf, S., et al. (2022). SARS-CoV-2 Omicron is an immune escape variant with an altered cell entry pathway. Nature Microbiology *7*, 1161-1179. 10.1038/s41564-022-01143-7.

Yang, S., Yu, Y., Jian, F., Song, W., Yisimayi, A., Chen, X., Xu, Y., Wang, P., Wang, J., Yu, L., et al. (2023). Antigenicity and infectivity characterisation of SARS-CoV-2 BA.2.86. The Lancet Infectious Diseases. https://doi.org/10.1016/S1473-3099(23)00573-X.

Yousefi, M., Lee, W.S., Chan, W.O.Y., He, W., Mah, M.G., Yong, C.L., Deerain, J.M., Wang, L., Arcinas, C., Yan, B., et al. (2023). Betacoronaviruses SARS-CoV-2 and HCoV-OC43 infections in IGROV-1 cell line require aryl hydrocarbon receptor. Emerging Microbes & Infections *12*, 2256416. 10.1080/22221751.2023.2256416.

Yue, C., Song, W., Wang, L., Jian, F., Chen, X., Gao, F., Shen, Z., Wang, Y., Wang, X., and Cao, Y. (2023). Enhanced transmissibility of XBB.1.5 is contributed by both strong ACE2 binding and antibody evasion. Biorxiv, 2023.2001.2003.522427. 10.1101/2023.01.03.522427.

a.

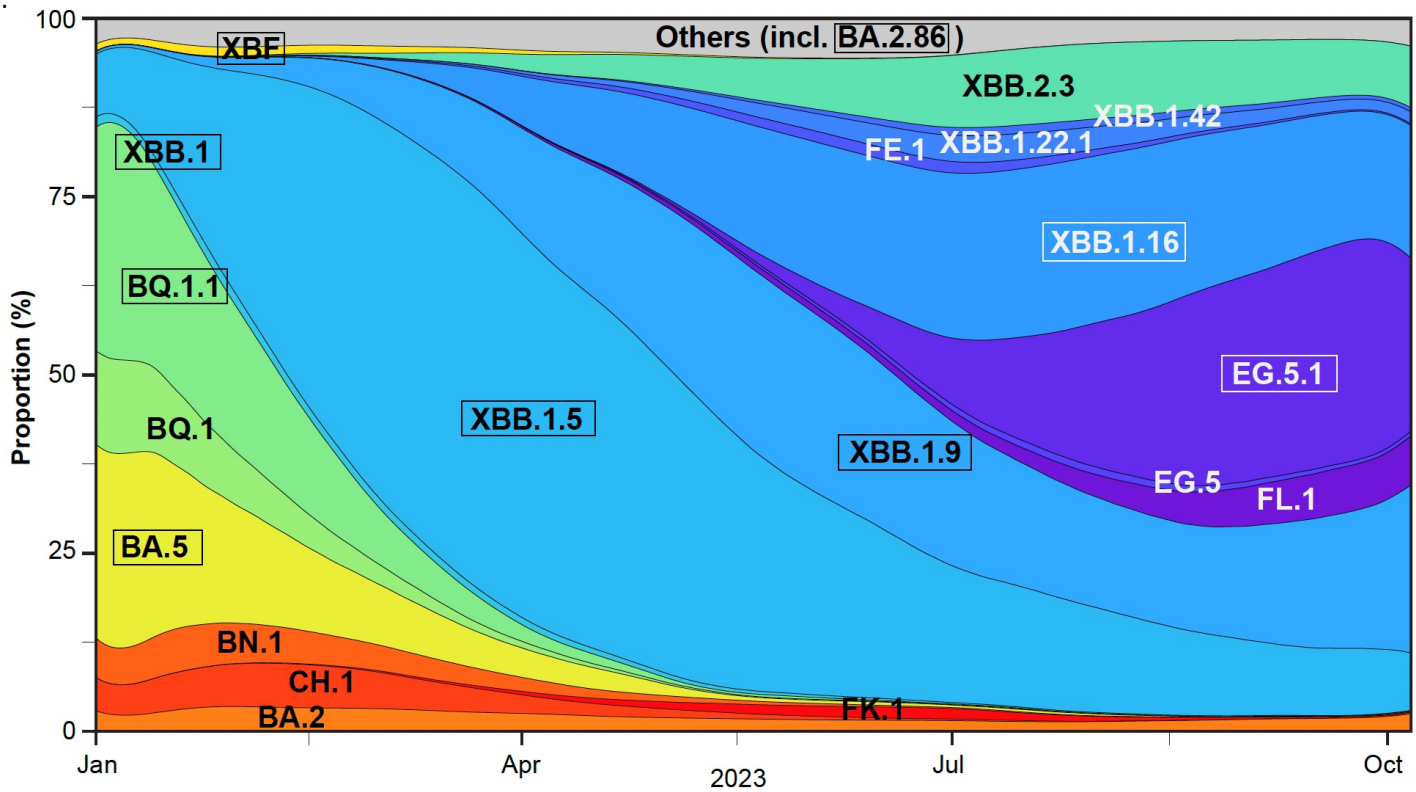
Others (incl. BA.2.86)
XBF
XBB.2.3
XBB.1.42
FE.1
XBB.1.22.1
XBB.1
XBB.1.16
BQ.1.1
EG.5.1
BQ.1
XBB.1.5
XBB.1.9
EG.5
FL.1
BA.5
BN.1
CH.1
BA.2
FK.1
Proportion (%)
100
75
50
25
0
Jan
Apr
2023
Jul
Oct

b.

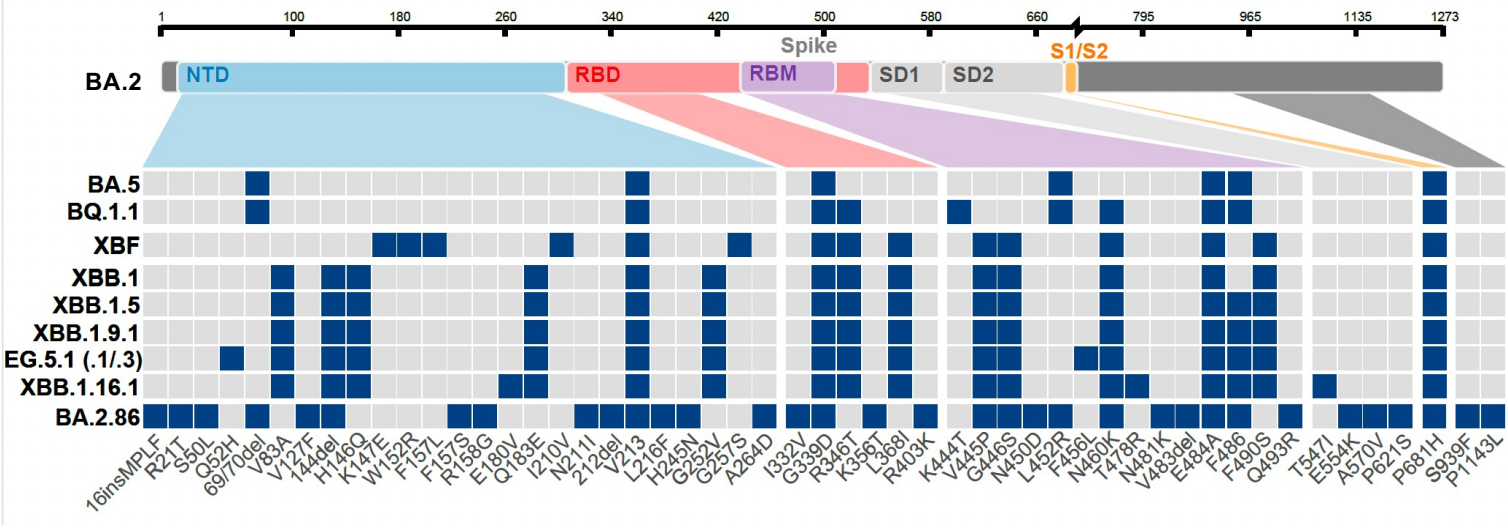
Spike
S1/S2
BA.2
NTD
RBD
RBM
SD1
SD2
BA.5
BQ.1.1
XBF
XBB.1
XBB.1.5
XBB.1.9.1
EG.5.1 (.1/.3)
XBB.1.16.1
BA.2.86
16insMPLF
R21T
S50L
Q52H
69/70del
V83A
V127F
144del
H146Q
K147E
W152R
F157L
F157S
R158G
E180V
Q183E
I210V
N211I
212del
V213
L216F
H245N
G252V
G257S
A264D
I332V
G339D
R346T
K356T
L368I
R403K
K444T
V445P
G446S
N450D
L452R
F456L
N460K
T478R
N481K
V483del
E484A
F486
F490S
Q493R
T547I
E554K
A570V
P621S
P681H
S939F
P1143L

Figure 1

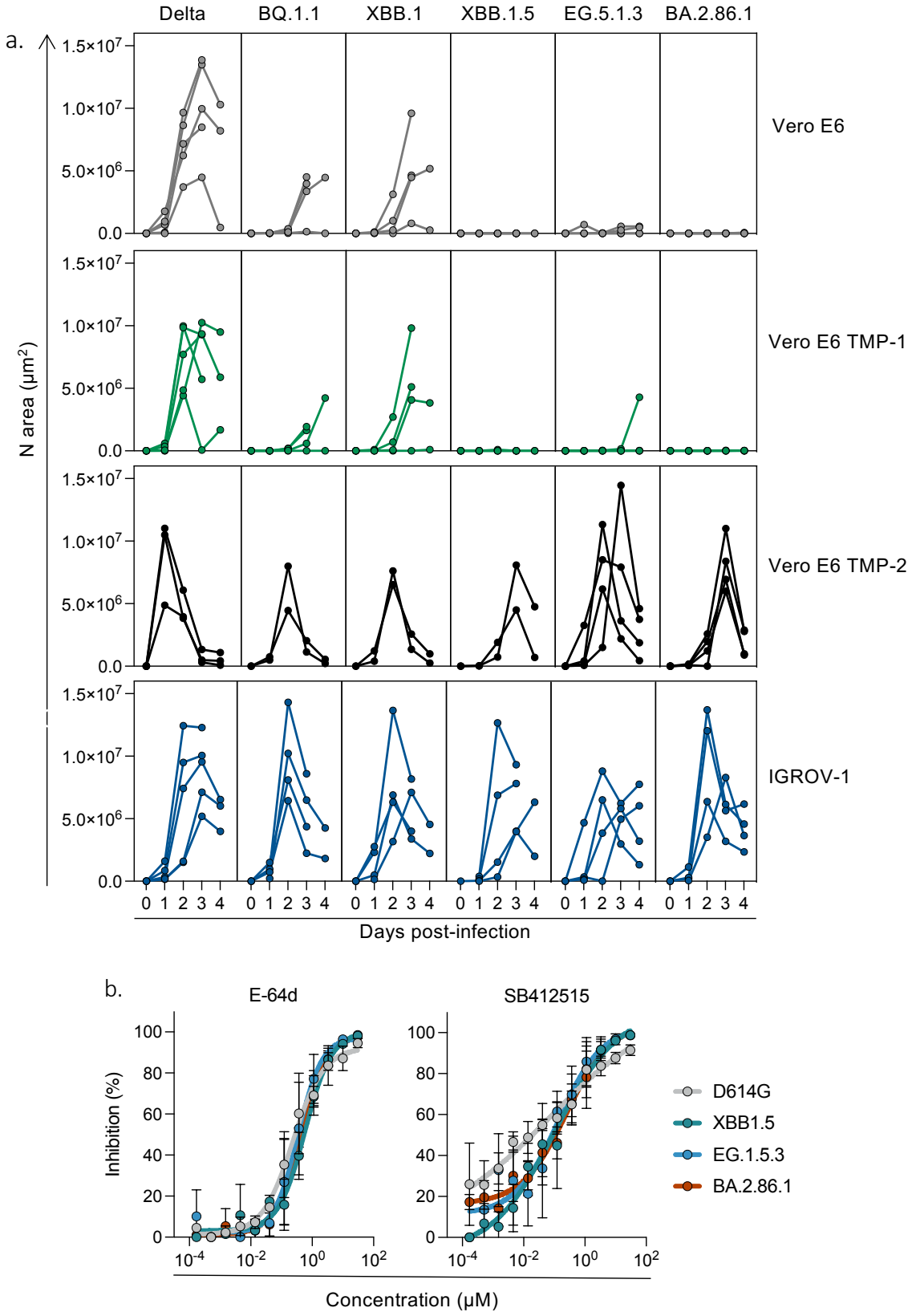
a.
Delta
BQ.1.1
XBB.1
XBB.1.5
EG.5.1.3
BA.2.86.1
Vero E6
Vero E6 TMP-1
Vero E6 TMP-2
IGROV-1
N area (μm²)
1.5×10⁷
1.0×10⁷
5.0×10⁶
0.0
0 1 2 3 4
Days post-infection
b.
E-64d
SB412515
Inhibition (%)
100
80
60
40
20
0
10⁻⁴
10⁻²
10⁰
10²
Concentration (μM)
D614G
XBB1.5
EG.1.5.3
BA.2.86.1

Figure 2

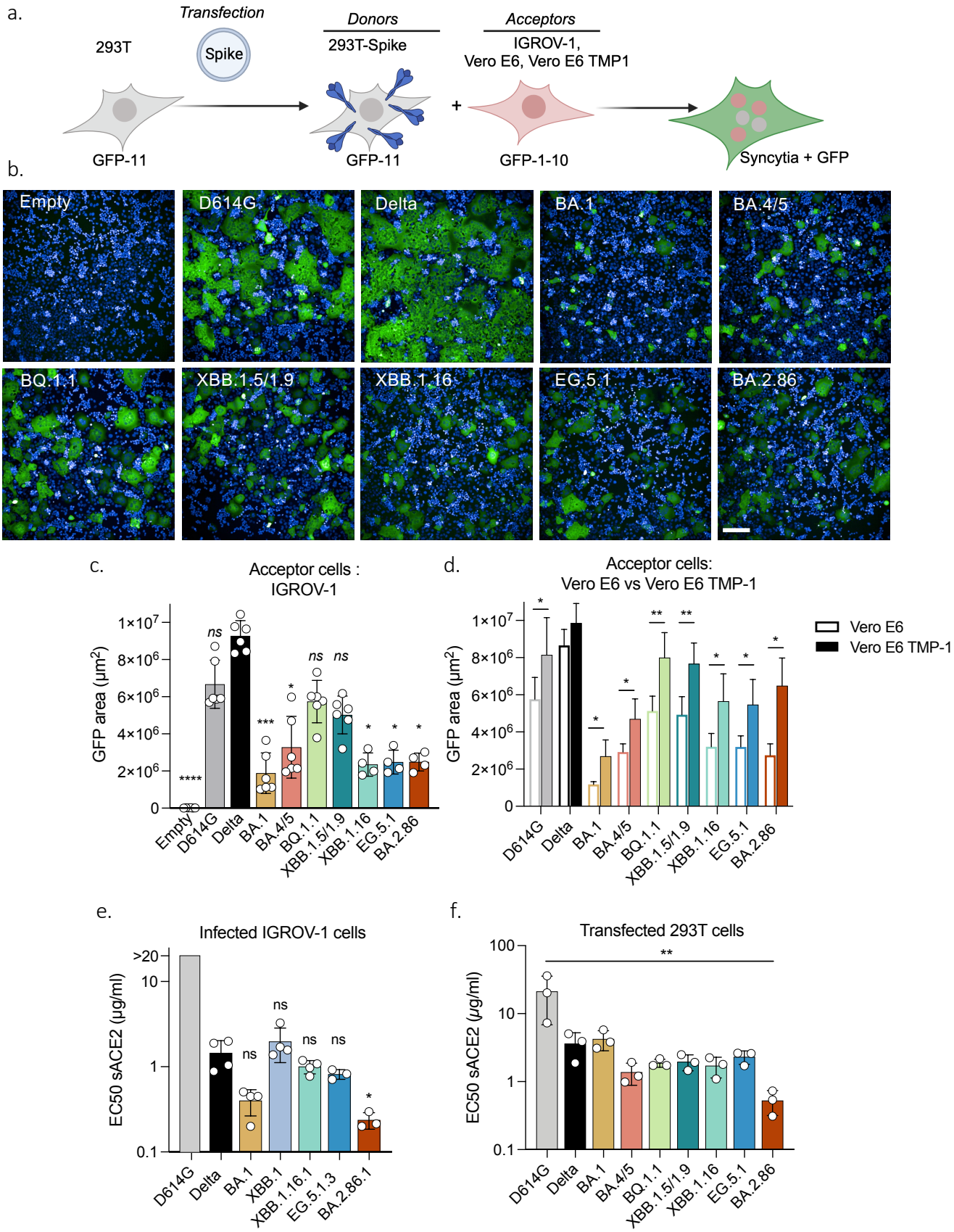
a.
Transfection
293T
Spike
GFP-11
Donors
293T-Spike
GFP-11
Acceptors
IGROV-1,
Vero E6, Vero E6 TMP1
+
GFP-1-10
Syncytia + GFP
b.
Empty
D614G
Delta
BA.1
BA.4/5
BQ.1.1
XBB.1.5/1.9
XBB.1.16
EG.5.1
BA.2.86
c.
Acceptor cells :
IGROV-1
GFP area (µm²)
1×10⁷
8×10⁶
6×10⁶
4×10⁶
2×10⁶
0
****
ns
***
*
ns
ns
*
*
*
Empty
D614G
Delta
BA.1
BA.4/5
BQ.1.1
XBB.1.5/1.9
XBB.1.16
EG.5.1
BA.2.86
d.
Acceptor cells:
Vero E6 vs Vero E6 TMP-1
Vero E6
Vero E6 TMP-1
GFP area (µm²)
1×10⁷
8×10⁶
6×10⁶
4×10⁶
2×10⁶
0
*
*
*
**
**
*
*
*
D614G
Delta
BA.1
BA.4/5
BQ.1.1
XBB.1.5/1.9
XBB.1.16
EG.5.1
BA.2.86
e.
Infected IGROV-1 cells
EC50 sACE2 (µg/ml)
>20
10
1
0.1
ns
ns
ns
ns
*
D614G
Delta
BA.1
XBB.1
XBB.1.16.1
EG.5.1.3
BA.2.86.1
f.
Transfected 293T cells
EC50 sACE2 (µg/ml)
100
10
1
0.1
**
D614G
Delta
BA.1
BA.4/5
BQ.1.1
XBB.1.5/1.9
XBB.1.16
EG.5.1
BA.2.86

Figure 3

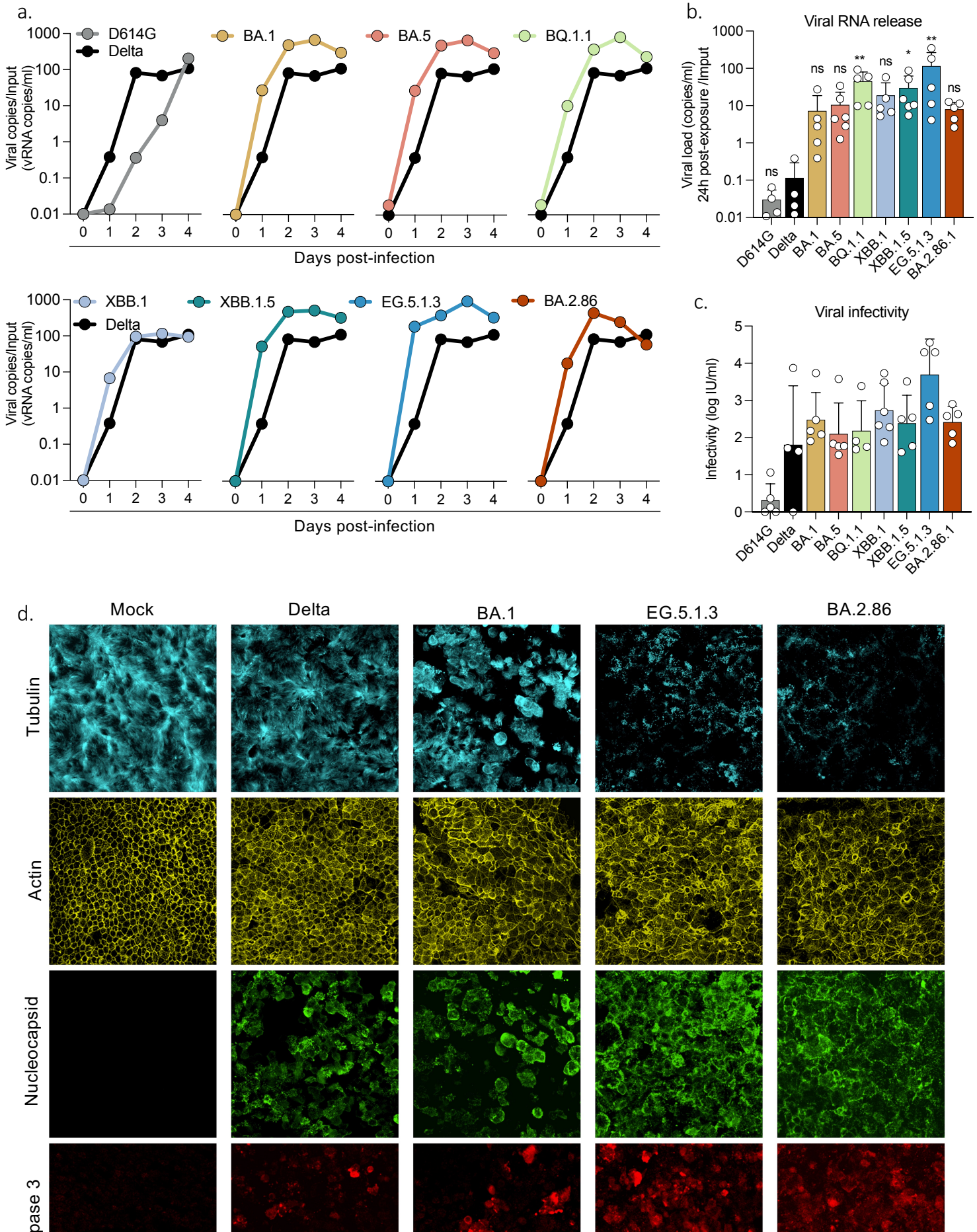
a.
D614G
Delta
BA.1
BA.5
BQ.1.1
Viral copies/Input (vRNA copies/ml)
Days post-infection
XBB.1
XBB.1.5
EG.5.1.3
BA.2.86
b.
Viral RNA release
Viral load (copies/ml) 24h post-exposure /Imput
ns
*
**
c.
Viral infectivity
Infectivity (log IU/ml)
d.
Mock
Delta
BA.1
EG.5.1.3
BA.2.86
Tubulin
Actin
Nucleocapsid
Caspase 3

Figure 4

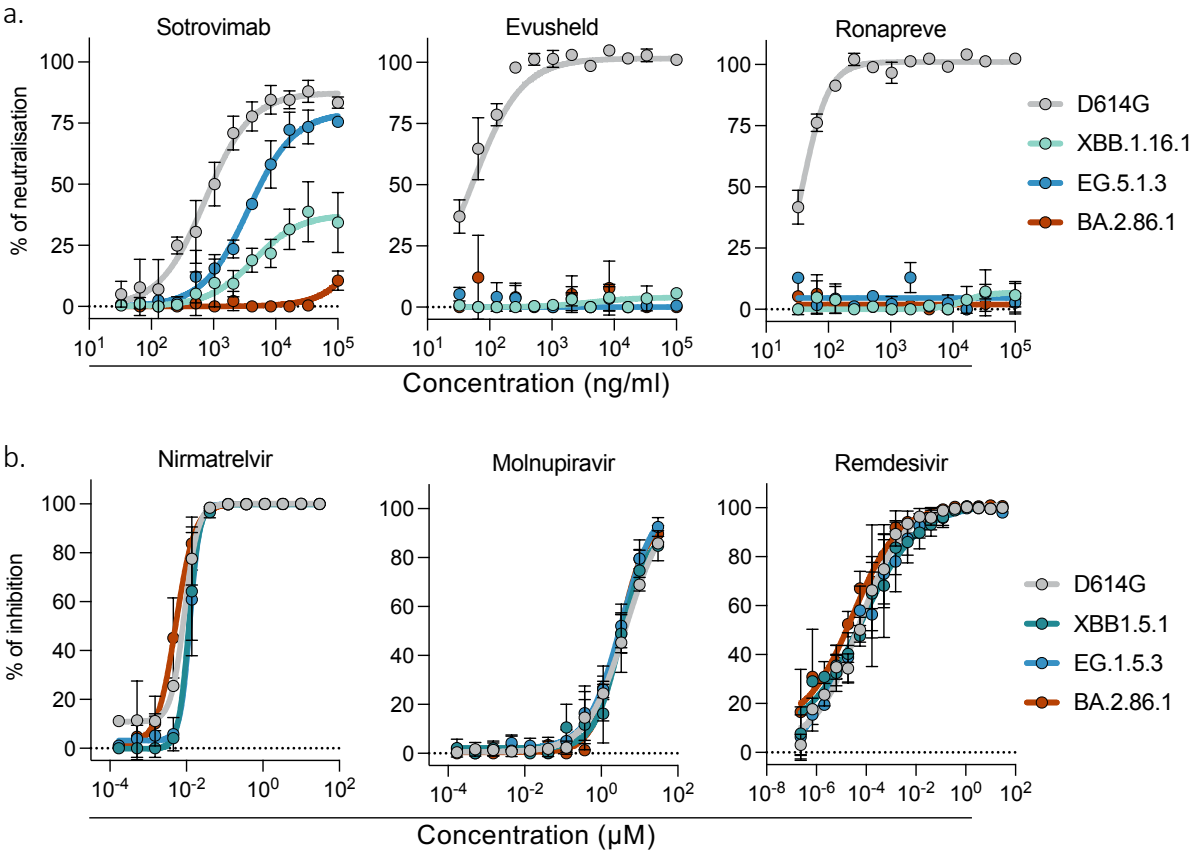
a.
Sotrovimab
Evusheld
Ronapreve
% of neutralisation
Concentration (ng/ml)
D614G
XBB.1.16.1
EG.5.1.3
BA.2.86.1
b.
Nirmatrelvir
Molnupiravir
Remdesivir
% of inhibition
Concentration (μM)
D614G
XBB1.5.1
EG.1.5.3
BA.2.86.1

Figure 5

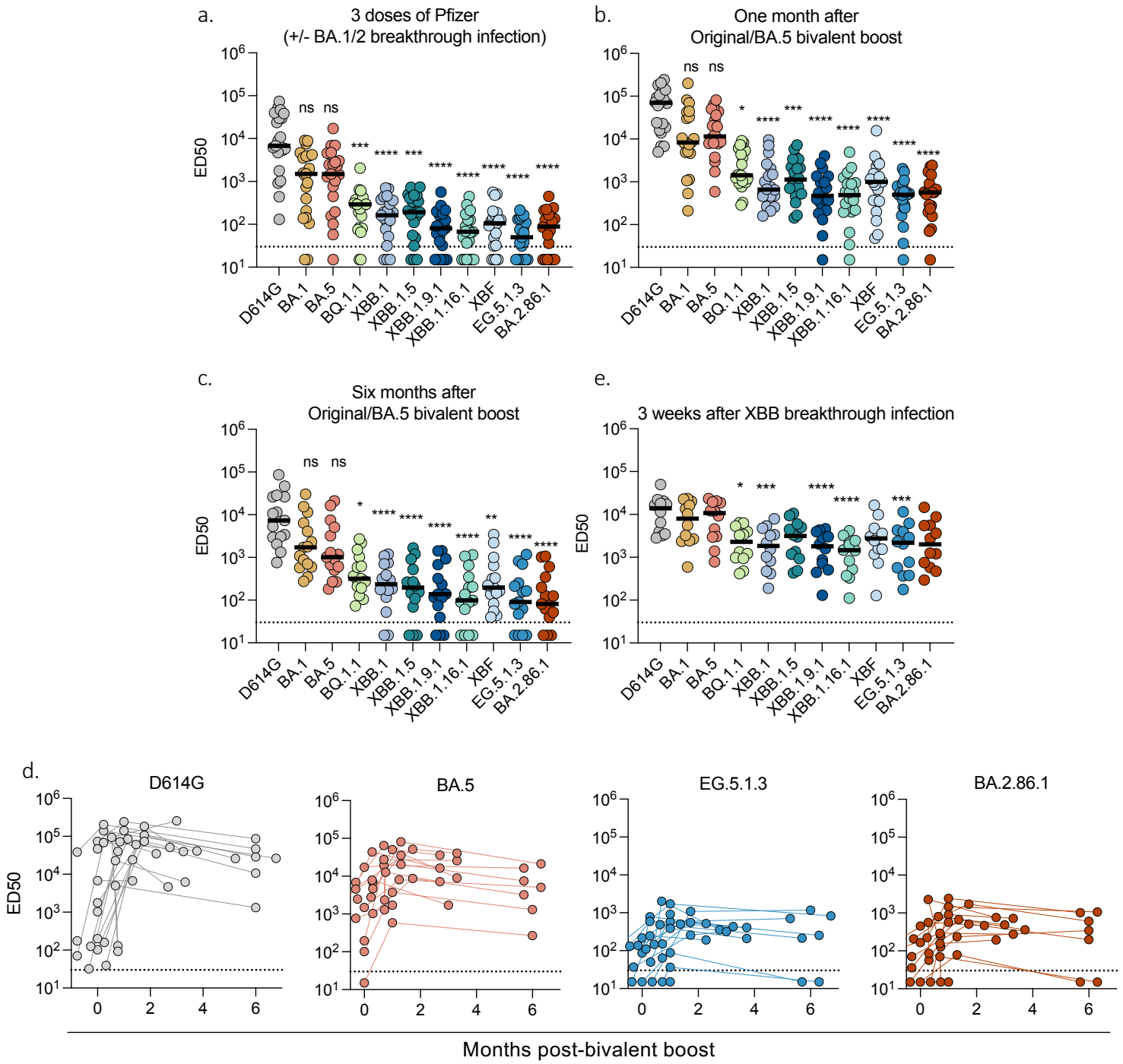
a.
3 doses of Pfizer
(+/- BA.1/2 breakthrough infection)
b.
One month after
Original/BA.5 bivalent boost
c.
Six months after
Original/BA.5 bivalent boost
e.
3 weeks after XBB breakthrough infection
ED50
D614G
BA.1
BA.5
BQ.1.1
XBB.1
XBB.1.5
XBB.1.9.1
XBB.1.16.1
XBF
EG.5.1.3
BA.2.86.1
ns
d.
D614G
BA.5
EG.5.1.3
BA.2.86.1
Months post-bivalent boost

Figure 6